

Supplemental Materials

Mathematical Modeling Reveals Quantitative Properties of KEAP1-NRF2 Signaling

Shengnan Liu, Jingbo Pi, and Qiang Zhang

Results for Models 1 and 2 3

Figures

• Figure S1. Dynamical and steady-state behaviors of Model 1.....	8
• Figure S2. Additional dynamical and steady-state behaviors of Model 1.....	9
• Figure S3. Dynamical and steady-state behaviors of Model 2.....	10
• Figure S4. Additional dynamical and steady-state behaviors of Model 2.....	12
• Figure S5. Additional dynamical and steady-state behaviors of Model 3a.....	13
• Figure S6. Effects of parameters k_1 (k'_1) on NRF2 responses in Model 3a.....	14
• Figure S7. Effects of parameters $k_{1,1}$ ($k'_{1,1}$) and $k_{2,1}$ ($k'_{2,1}$) on NRF2 responses in Model 3a.....	15
• Figure S8. Effects of parameters k_3 (k'_3) on NRF2 responses in Model 3a.....	18
• Figure S9. Effects of varying parameter k'_3 alone on NRF2 responses in Model 3a to test hinge-latch hypothesis.....	19
• Figure S10. Effects of varying parameter k_7 and k_8 on NRF2 responses in Model 3a.....	20
• Figure S11. Effects of total KEAP1 abundance on NRF2 responses in Model 3a.....	21
• Figure S12. Dynamical changes of various NRF2 species in Model 3b in response to a high $CLASS_{VI}$ level.....	22
• Figure S13. Dynamical changes of various NRF2 species in Model 4a in response to different $CLASS_{IV}$ levels.....	23
• Figure S14. Effects of total nuclear KEAP1 abundance on the steady-state dose-response curves of various NRF2 species in Model 4a.....	24
• Figure S15. Effects of basal total nuclear NRF2 abundance on steady-state dose-response of various NRF2 species in Model 4a.....	25
• Figure S16. Effects of varying parameter k_7 and k_8 on NRF2 responses in Model 4a.....	26
• Figure S17. Effects of total nuclear KEAP1 abundance on the steady-state dose-response curves of various NRF2 species in Model 4b.....	29
• Figure S18. Effects of basal total nuclear NRF2 abundance on steady-state dose-response of various NRF2 species in Model 4b.....	30

Tables

• Table S1. Model Parameters, Default Values, Sources and Justifications.....	31
• Table S2. ODEs of Models 1 and 2.....	36
• Table S3. ODEs of Model 3a.....	37
• Table S4. ODEs of Model 3b.....	38
• Table S5. ODEs of Model 4a.....	39
• Table S6. ODEs of Model 4b.....	41
• Table S7. Algebraic equations.....	43
• Table S8. Basal steady-state concentrations of NRF2 and KEAP1 species.....	44

• Table S9. Maximally induced steady-state concentrations of NRF2 and KEAP1 species	44
• Table S10. Basal turnover fluxes of KEAP1-NRF2 models	44
• Table S11. Maximally-induced turnover fluxes of KEAP1-NRF2 models	44
• Table S12. Classes of electrophilic and non-electrophilic NRF2 activators	45
<u>References</u>	46

Results for Models 1 and 2

Model 1 (Equilibrium Mode)

Model 1 is the minimal model, involving only basic cytosolic KEAP1 and NRF2 interactions through ETGE and DLG motifs (Fig. 1). At the basal steady state, due to the strong binding between KEAP1 and NRF2 through ETGE, the majority of NRF2 is sequestered by KEAP1, leaving *free NRF2* ($NRF2_{free}$), at 2 nM, just a tiny fraction of *total NRF2* ($NRF2_{tot}$), which is at 150 nM (Fig. S1A and Table S8). The open state of the KEAP1-NRF2 complex ($KEAP1_NRF2_{open}$), in which the association is through ETGE only, and the closed state of the complex ($KEAP1_NRF2_{closed}$), in which the association is through both ETGE and DLG, are equal to each other in concentration at 74 nM and much higher than $NRF2_{free}$. The comparable levels between the open and closed states are consistent with what was observed experimentally in HEK293 cells (Baird et al. 2013). When the synthesis of NRF2 is terminated by setting $k_0=0$, all NRF2 species including $NRF2_{free}$, $KEAP1_NRF2_{open}$ and $KEAP1_NRF2_{closed}$, degrade exponentially, and the half-life of $NRF2_{tot}$ is 10 min (Fig. S1A).

To examine the basic behavior of the model when NRF2 in $KEAP1_NRF2_{closed}$ is stabilized, as would occur during oxidative stress, we first lowered k_6 to different values, while keeping *class I-V activator* at zero ($CLASS_{I-V}=0$) for simplicity. As k_6 decreases from the default $2.03E-3\ S^{-1}$ (equivalent half-life $t_{1/2}=5.7$ min for $KEAP1_NRF2_{closed}$) to $1.178E-4$ (which is the default value of k'_6 for degradation of $KEAP1_NRF2_{closed}$, equivalent $t_{1/2}=98$ min), all NRF2 species increase and reach steady states in about 300 min (Fig. S1B). $KEAP1_NRF2_{open}$ and $KEAP1_NRF2_{closed}$ reach the steady states the fastest, followed by $NRF2_{free}$ and $NRF2_{tot}$. There is an apparent delay in the $NRF2_{free}$ response. $NRF2_{tot}$ increases by 5-fold, from 150 to 750 nM, while $NRF2_{free}$ increases by a much greater fold, from 2 to 230 nM. At this activated state, by setting $k_0=0$, all NRF2 species degrade but at different rates with $NRF2_{free}$ disappearing much more quickly, and the half-life of $NRF2_{tot}$ is 54 min (Fig. S1B). By setting k_6 to an even lower value ($0.589E-4$), the steady-state levels of both $NRF2_{free}$ and $NRF2_{tot}$ increase but only to a limited extent, and the half-life of $NRF2_{tot}$ lengthens to 65 min (Fig. S2A). When k_6 is lowered to zero, mimicking complete shutoff of KEAP1-mediated NRF2 degradation, $NRF2_{tot}$ only increases to 858 nM, a 5.7-fold increase from the basal level and its half-life lengthens to 78 min, while $NRF2_{free}$ increases by 117-fold (Fig. S2C). The behavior when $k_6=0$ represents the maximal response Model 1 can be induced. We next examined the steady-state dose-response behavior of Model 1 by varying the $CLASS_{I-V}$ level. With k'_6 at the default value, $NRF2_{free}$ exhibits an ultrasensitive, sigmoidal dose-response with Hill

coefficient (n_H) of 2.02 and maximal local response coefficient (LRC_{max}) of 1.92 (Figs. S1C in dual-log scale and S1D in dual-linear scale). $NRF2_{tot}$ is subsensitive with a much shallower dose-response curve. Setting k'_6 to lower values increases the ultrasensitivity of $NRF2_{free}$ slightly as its maximal steady-state level increases (Figs. S2B and S2D).

An interesting feature of Model 1 is that the open and closed KEAP1-NRF2 complexes ($KEAP1_NRF2_{open}$ and $KEAP1_NRF2_{closed}$) behave in an almost synchronized fashion in that their abundance ratio remains at 1:1 at all times in all conditions (Figs. S1A-S1C and S2), suggesting these two species are always at equilibrium to each other. Using FRET to track the open and closed states of KEAP1-NRF2 complex, Baird et al. observed that the two states diverge and do not follow an equilibrium mode of operation in a variety of chemically perturbed conditions (Baird et al. 2013). But rather, a “cyclic sequential attachment and regeneration” (abbreviated as “cycle”) mode of operation was suggested. In this mode, because of the rapid degradation of NRF2 in the closed KEAP1-NRF2 complex, KEAP1 is quickly released (or regenerated) to join the free KEAP1 dimer pool and sequester newly synthesized NRF2 again, thus completing a global cycle for KEAP1. Under oxidative stress, this cycle is blocked as the NRF2 degradation-coupled release of KEAP1 from the closed KEAP1-NRF2 complex is inhibited, leading to accumulation of the closed state and depletion of free KEAP1 dimer. Therefore, in the next section, we evolved Model 1 into Model 2 such that the model behavior is aligned with the cycle mode of operation.

Model 2 (Cycle Mode)

Examining the basal steady-state behaviors of Model 1 revealed that the two fluxes of the reversible conversion between $KEAP1_NRF2_{open}$ and $KEAP1_NRF2_{closed}$ are comparable to each other ($flux_{k_3} = 14.645$ and $flux_{k_4} = 14.495$ nM/S) and overwhelmingly dominant over the connected turnover fluxes (> 96 -fold of $flux_{k_6}$ and $flux_{k_9}$) (Table S10). The predominantly high $flux_{k_3}$ and $flux_{k_4}$ explain why the open and closed KEAP1-NRF2 complexes in Model 1 behave in an equilibrium mode of operation. To convert it to a cycle mode, we reduced the parameter values of k_3 and k_4 . When k_4 is reduced to about $1.96E-4$ S⁻¹ or lower (simultaneously reducing k_3 to keep the open:closed ratio at 1:1 at the basal condition), the behaviors of $KEAP1_NRF2_{open}$ and $KEAP1_NRF2_{closed}$ start to separate appreciably. As detailed in Table S1 footnote, Model 2 was finally configured with $k_4=1.0E-4$ as the default value and k_0 , k_3 and k_6 adjusted accordingly to maintain the same basal $NRF2_{tot}$ level and half-life as Model 1. As a result, the basal $flux_{k_3} = 0.135$, $flux_{k_4} = 7.35E-3$, and $flux_{k_6} = 0.128$ nM/S approximately (Table S10), indicating that the majority of NRF2 moving from the open to closed state through the k_3 step is degraded within

$KEAP1_NRF2_{\text{closed}}$ through the k_6 step, and only a small fraction (5.5%) returns to the open state through the k_4 step.

Fig. S3A shows the behaviors of NRF2 species decaying from the basal steady state when setting $k_0=0$. While the half-life of $NRF2_{\text{tot}}$ is still 10 min, the levels of $KEAP1_NRF2_{\text{open}}$ and $KEAP1_NRF2_{\text{closed}}$ diverge quickly with the open state decaying much faster than the closed state. By 15 min the open:closed ratio is about 1:2.7, comparable to what was observed in HEK293 cells treated with cycloheximide (Baird et al. 2013). By setting k_4 to lower values than the default and in the extreme case $k_4=0$ such that the binding between KEAP1 and DLG becomes irreversible (and k_0 , k_3 and k_6 were adjusted accordingly as above), the divergent behaviors of $KEAP1_NRF2_{\text{open}}$ and $KEAP1_NRF2_{\text{closed}}$ are similar to Fig. S3A (simulation results not shown).

To examine the basic behavior of the model when NRF2 in $KEAP1_NRF2_{\text{closed}}$ is stabilized, k_6 was lowered to different values, while keeping $CLASS_{i-v}=0$. As k_6 decreases from the default $1.74E-3 \text{ S}^{-1}$ (equivalent $t_{1/2}=5.7 \text{ min}$) to $1.454E-4$ (which is the default value of k'_6 , equivalent $t_{1/2}=79 \text{ min}$), all NRF2 species reach steady states in about 400 min (Fig. S3B). $KEAP1_NRF2_{\text{open}}$ and $KEAP1_NRF2_{\text{closed}}$ quickly diverge with $KEAP1_NRF2_{\text{closed}}$ increasing and reaching the steady state in about 100 min, while $KEAP1_NRF2_{\text{open}}$ initially increases slightly but then decreases to a level slightly lower than the basal level. The open:closed ratio decreases and reaches about 1:4.6 at 1 h, concordant with what was observed experimentally in HEK293 cells treated with proteasomal inhibitor MG132 or chemical stressors such as sulforaphane and sulfoxothiobamylate alkyne (Baird et al. 2013). $NRF2_{\text{tot}}$ increases from 150 to 750 nM, while $NRF2_{\text{free}}$ increases by a much greater fold, from 2 to 223 nM. At this activated state, by setting $k_0=0$, all NRF2 species degraded, with a half-life of 68.5 min for $NRF2_{\text{tot}}$, while $NRF2_{\text{free}}$ seems to disappear much more quickly approaching the zero level within 1 h (Fig. S3B). By setting k_6 to even lower values, the maximal levels of both $NRF2_{\text{free}}$ and $NRF2_{\text{tot}}$ increase but to a limited extent and the half-life of $NRF2_{\text{tot}}$ lengthens to 191 min in the extreme case when $k_6=0$ (Figs. S4A and S4C). Interestingly, the decay of $NRF2_{\text{tot}}$ starts to become biphasic. The first fast phase is due to rapid $NRF2_{\text{free}}$ drop, and the second slow phase follows the decay of $KEAP1_NRF2_{\text{closed}}$.

We next examined the dynamical responses of Model 2 to a range of $CLASS_{i-v}$ levels. $NRF2_{\text{tot}}$ increases to higher steady-state levels with increasing $CLASS_{i-v}$ levels, and the time it takes to reach steady states also increases (Fig. S3C), which is concordant with the lengthening of the half-life as more NRF2 is diverted to the more stable, closed state complex. In comparison,

there is a considerable delay in the response of $NRF2_{free}$, which does not rise tangibly above the basal level until after 60 min (Fig. S3D). After the initial delay, the rising time of $NRF2_{free}$ becomes shorter with higher $CLASS_{i-v}$ levels. The initial delay is caused by the sequestration of newly synthesized NRF2 by *free KEAP1 dimer* ($KEAP1_{free}$), the level of which decreases quickly as it forms complexes with NRF2 (Fig. S3E).

The steady-state $NRF2_{free}$ level exhibits an ultrasensitive response with respect to $CLASS_{i-v}$ levels, with n_H of 2.62 and LRC_{max} of 3.09 (Fig. S3F). Interestingly, unlike steady-state $KEAP1_NRF2_{closed_tot}$ ($KEAP1_NRF2_{closed} + KEAP1_o_NRF2_{closed}$) which increases monotonically with $CLASS_{i-v}$ levels, steady-state $KEAP1_NRF2_{open_tot}$ ($KEAP1_NRF2_{open} + KEAP1_o_NRF2_{open}$) exhibits a nonmonotonic dose-response profile (Fig. S3F, green line). The peak coincides with the juncture of KEAP1 saturation at which point $KEAP1_{free}$ is nearly depleted and $NRF2_{free}$ increases sharply. The decrease in $KEAP1_NRF2_{open_tot}$ at higher $CLASS_{i-v}$ levels is due to increasing $flux_{k5}$ associated with increasing $NRF2_{free}$, which takes away from the net flux toward the KEAP1-NRF2 complexes (Table S11). When k'_6 is set to lower values, the degree of $NRF2_{free}$ ultrasensitivity is enhanced slightly, due to higher maximal $NRF2_{tot}$ and $NRF2_{free}$ levels that can be achieved (Figs. S4B and S4D), and the opposite occurs when k'_6 is high (Fig. S4F).

To analyze the mechanism of ultrasensitivity, we conducted flux analysis by artificially clamping $NRF2_{free}$ to different levels. $flux_{k5}$ increases linearly with the clamped $NRF2_{free}$ level, while $flux_{k9}$ and $flux_{k6}$ also increase but become saturated eventually because of the depletion of free KEAP1 dimer (Figs. 3G and 3H). The *total degradation rate* ($flux_{k5} + flux_{k6} + flux_{k9}$) exhibits an S-shape containing 3 phases. The initial rising phase is dominated by $flux_{k6}$ because k_6 is the highest compared with k_5 and k_9 and the closed state is higher in concentration. The second phase is slowly rising and nearly flat because of saturation of $flux_{k6}$ and to a small extent of $flux_{k9}$. The flatness of this second phase represents zero-order degradation, i.e., the *total degradation rate* is insensitive to changes in NRF2 levels. In the third phase, the *total degradation rate* rises again, because $flux_{k5}$ now becomes dominant. The intersection point between the *total degradation rate* and NRF2 *synthesis rate* ($flux_{k0}$) represents the steady state of $NRF2_{free}$. When $k_6=5.22E-4$ (30% of default value) to mimic a mild stress condition, the intersection point appears at the junction of the first and second phases and the corresponding $NRF2_{free}$ is about 4 nM (Fig. S3G). When k_6 is lowered further to $1.74E-4$ (10% of default) to mimic a more severe stress condition, the $flux_{k6}$ curve shifts to lower levels and as a result the second, flat phase of *total degradation rate* shifts downward as well (Fig. S3H). The intersection point between *total*

degradation rate and NRF2 *synthesis rate* swings dramatically to the right, at the junction of the second and third phase, resulting in a much higher steady-state level of $NRF2_{free}$ at 175 nM. Therefore, a remarkable signal amplification is evident here – as k_6 decreases by only 3-fold (from 30% to 10% of default value), $NRF2_{free}$ increases by 43-fold. In the meantime, the steady-state $NRF2_{tot}$ exhibits no ultrasensitivity, as it increases from 326 to 701 nM, a 2.2-fold change only.

Figures

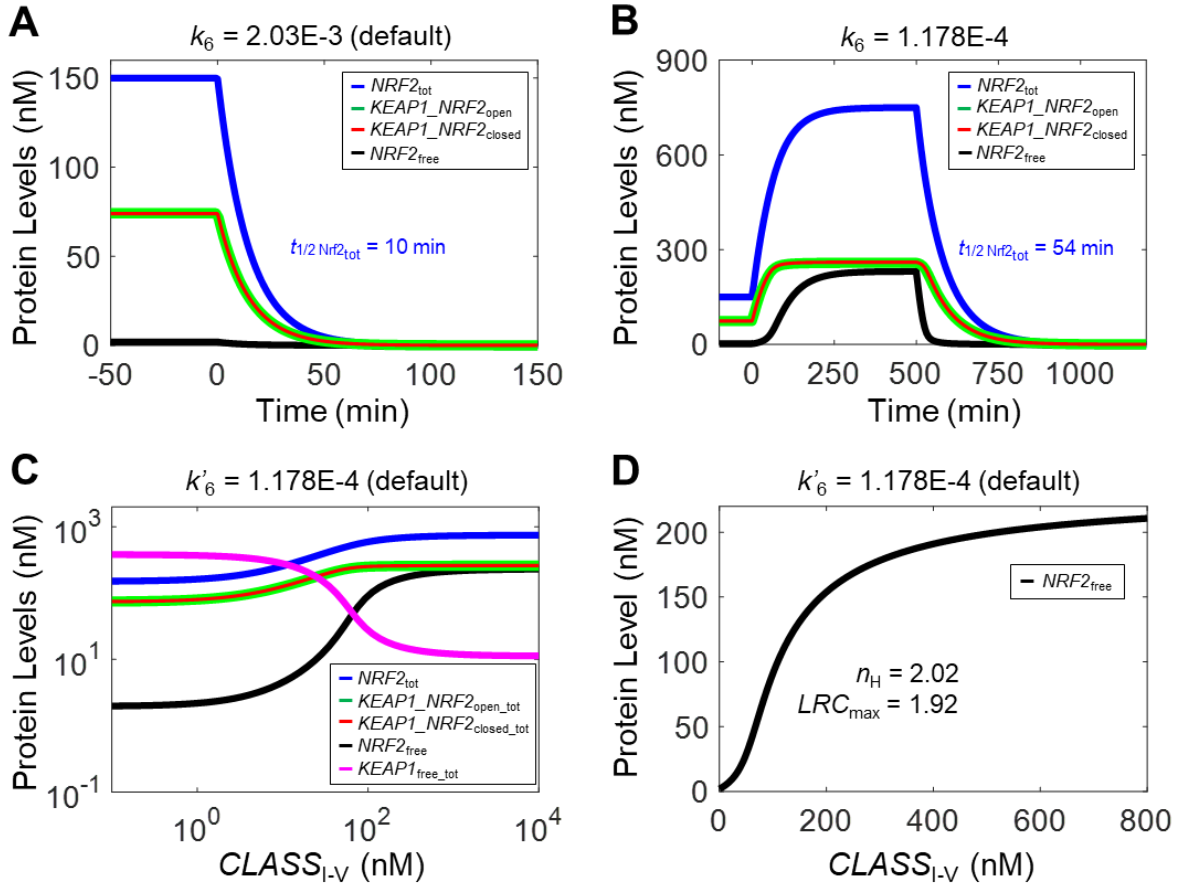


Figure S1. Dynamical and steady-state behaviors of Model 1. (A) Dynamical changes of basal $NRF2_{free}$, $KEAP1_NRF2_{open}$, $KEAP1_NRF2_{closed}$, and $NRF2_{tot}$ in response to termination of NRF2 synthesis (by setting $k_0=0$) starting at 0 min with k_6 at default value. (B) Dynamical changes of various NRF2 species in response to stabilization of NRF2 in $KEAP1_NRF2_{closed}$ by setting $k_6=1.178E-4$ starting at 0 min and in response to termination of NRF2 synthesis (by setting $k_0=0$) starting at 500 min. For simulations in (A) and (B), $CLASS_{I-V}$ level is kept at zero. (C) Steady-state dose-response curves of various NRF2 species and $KEAP1_{free}$ for $CLASS_{I-V}$ on dual-log scale with k'_6 at default value. n_H and LRC_{max} for $NRF2_{total}$ are 1.17 and 0.40 respectively (not shown). (D) Steady-state dose-response curves of $NRF2_{free}$ in (C) on dual-linear scale illustrating sigmoidal shape, with n_H and LRC_{max} indicated.

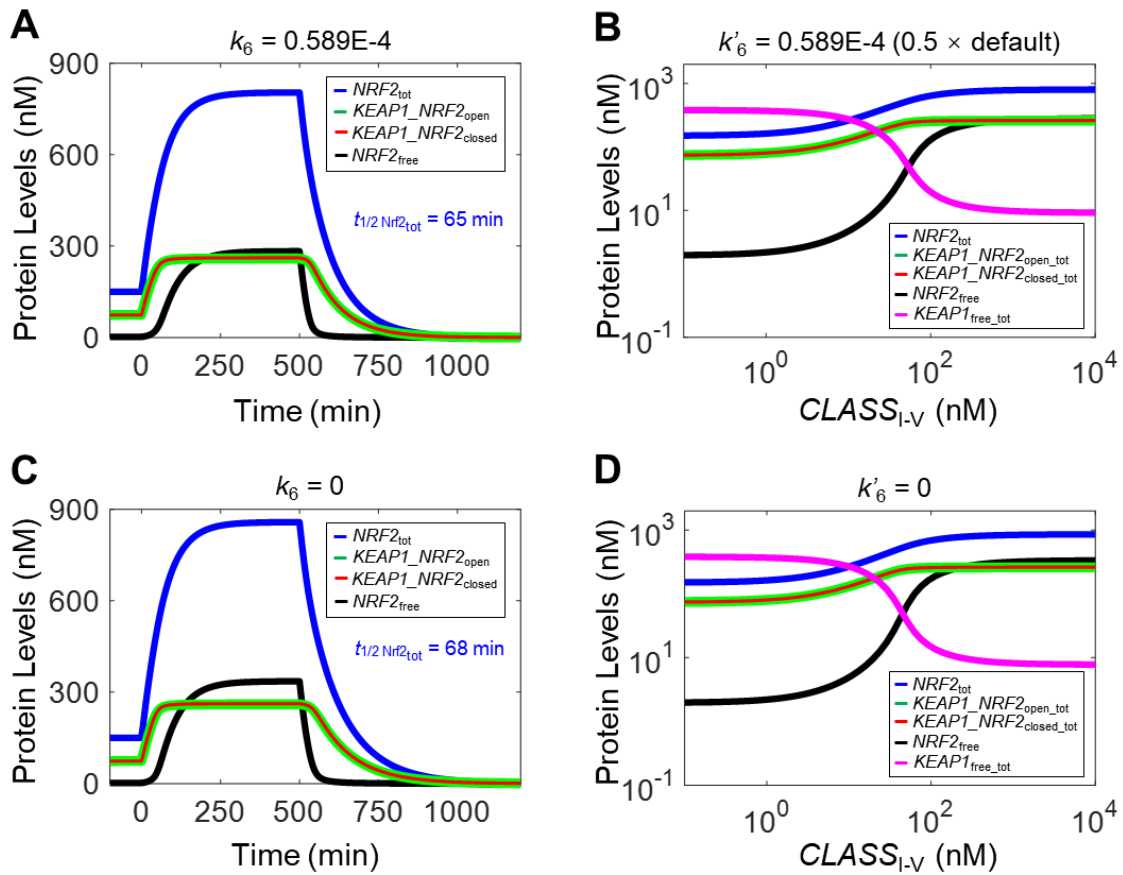


Figure S2. Additional dynamical and steady-state behaviors of Model 1. Dynamical changes of $\text{NRF2}_{\text{free}}$, $\text{KEAP1_NRF2}_{\text{open}}$, $\text{KEAP1_NRF2}_{\text{closed}}$, and NRF2_{tot} in response to stabilization of NRF2 in $\text{KEAP1_NRF2}_{\text{closed}}$ by setting (A) $k_6=0.589E-4$ and (C) $k_6=0$ starting at 0 min and in response to termination of NRF2 synthesis (by setting $k_0=0$) starting at 500 min. For simulations in (A) and (B), CLASS_{i-V} level is kept at zero. Steady-state dose-response curves of various NRF2 species and $\text{KEAP1}_{\text{free}}$ with (B) $k'_6=0.589E-4$ and (D) $k'_6=0$.

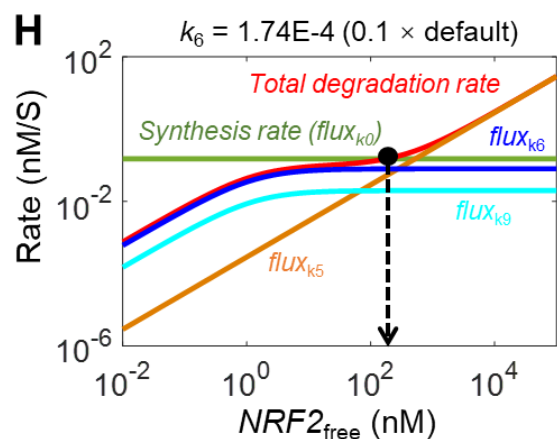
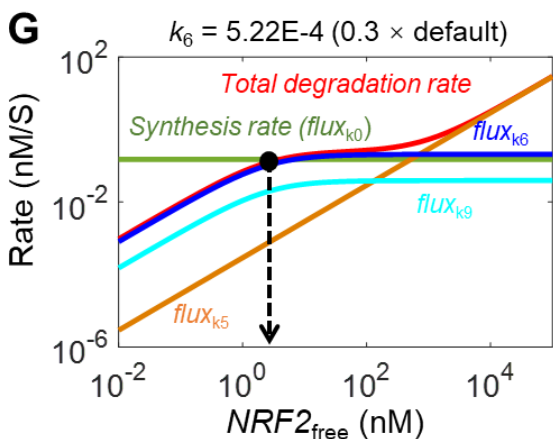
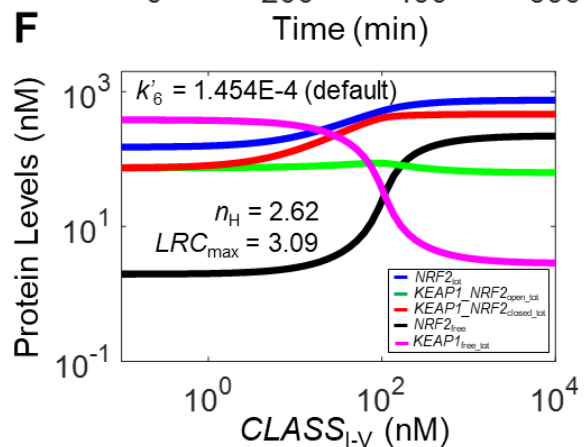
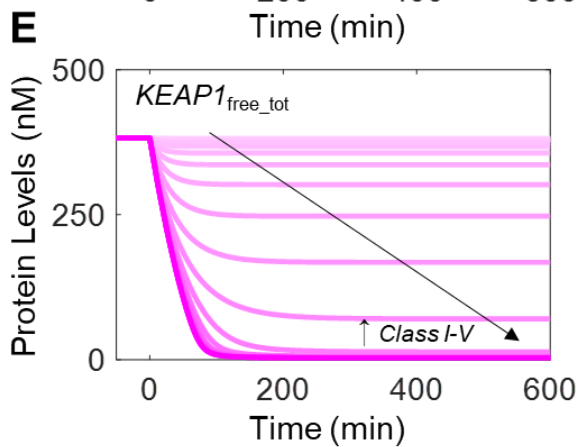
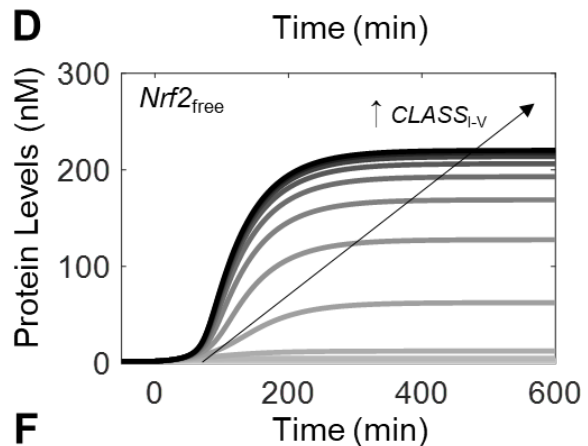
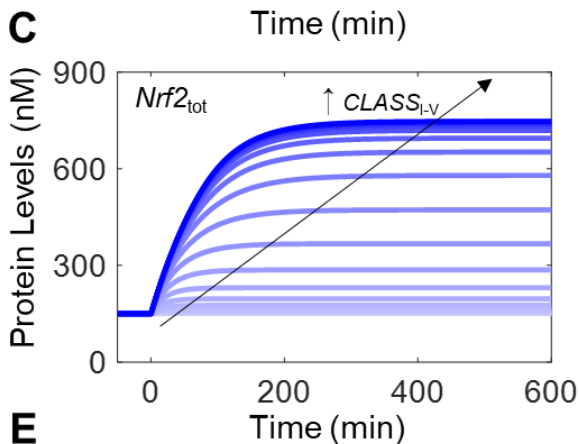
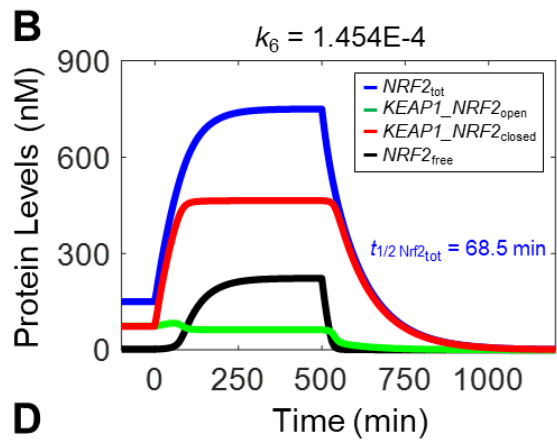
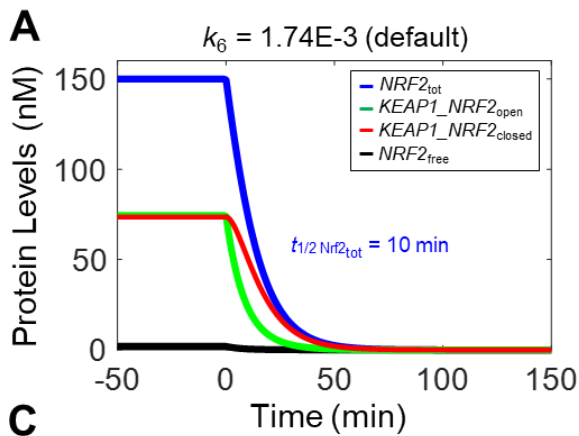


Figure S3. Dynamical and steady-state behaviors of Model 2. (A) Dynamical changes of basal $NRF2_{free}$, $KEAP1_NRF2_{open}$, $KEAP1_NRF2_{closed}$, and $NRF2_{tot}$ in response to termination of NRF2 synthesis (by setting $k_0=0$) starting at 0 min with k_6 at default value. (B) Dynamical changes of various NRF2 species in response to stabilization of NRF2 in $KEAP1_NRF2_{closed}$ by setting $k_6=1.454E-4$ starting at 0 min and in response to termination of NRF2 synthesis (by setting $k_0=0$) starting at 500 min. For simulations in (A) and (B), $CLASS_{i-v}$ level is kept at zero. (C-E) Dynamical changes of $NRF2_{tot}$ (C), $NRF2_{free}$ (D), and $KEAP1_{free_tot}$ ($KEAP1_{free}+KEAP1_{o_{free}}$) (E) in response to different levels of $CLASS_{i-v}$ (ranging from 0.1 to 1E4 nM) with k'_6 at default value. (F) Steady-state dose-response curves of various NRF2 species and $KEAP1_{free_tot}$ on double-log scale with k'_6 at default value. Shown are n_H and LRC_{max} for $NRF2_{free}$; n_H and LRC_{max} for $NRF2_{total}$ are 1.27 and 0.42 respectively (not shown). (G-H) Flux analyses for conditions when NRF2 in $KEAP1_NRF2_{closed}$ is stabilized by setting k_6 to 30% (G) and 10% (H) of default value.

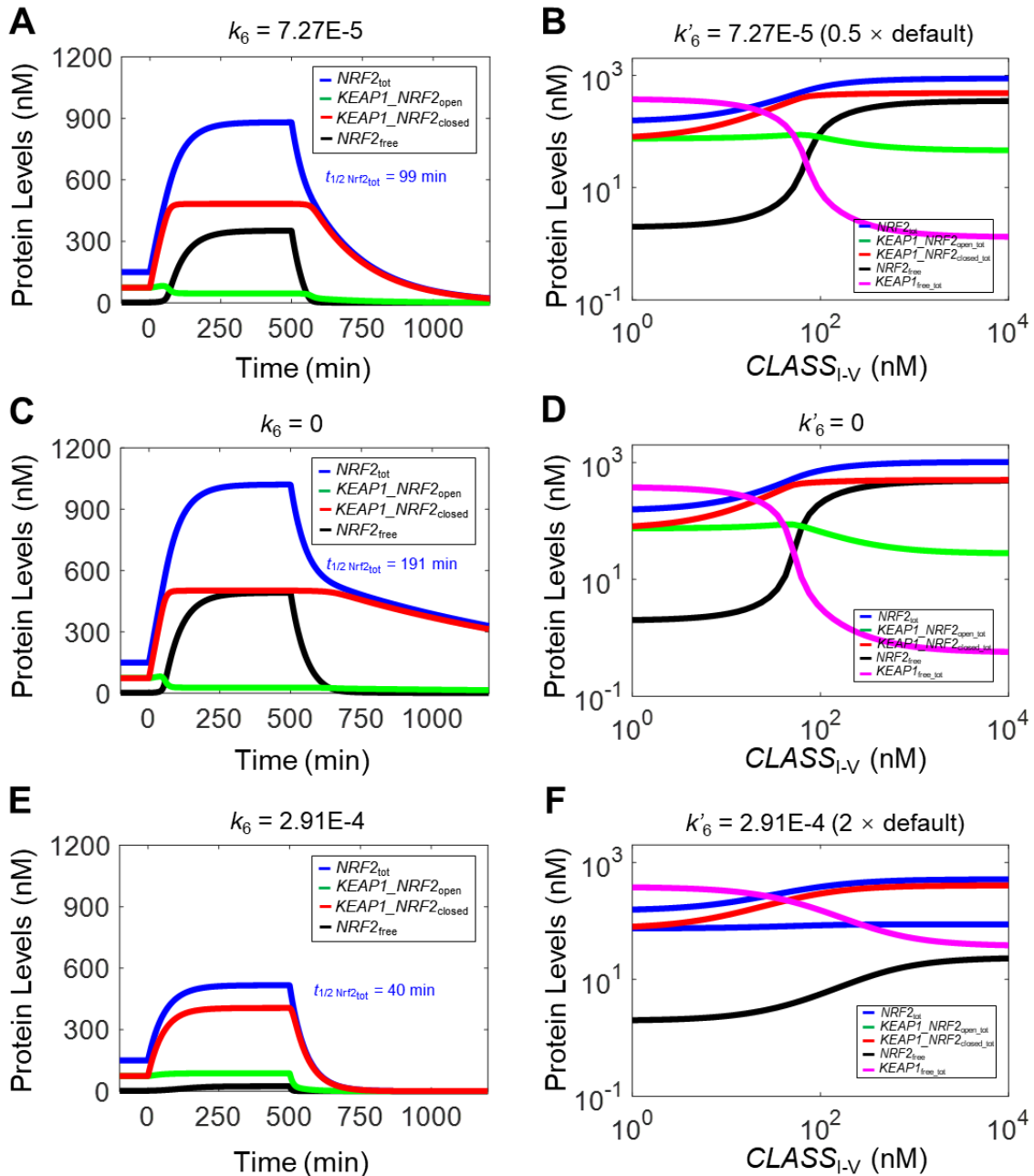


Figure S4. Additional dynamical and steady-state behaviors of Model 2. Dynamical changes of $NRF2_{free}$, $KEAP1_NRF2_{open}$, $KEAP1_NRF2_{closed}$, and $NRF2_{tot}$ in response to stabilization of $NRF2$ in $KEAP1_NRF2_{closed}$ by setting (A) $k_6=7.27E-5$, (C) $k_6=0$, and (E) $k_6=2.91E-4$ starting at 0 min and in response to termination of $NRF2$ synthesis (by setting $k_0=0$) starting at 500 min. For simulations in (A, C, and E), $CLASS_{I-V}$ level is kept at zero. Steady-state dose-response curves of various $NRF2$ species and $KEAP1_{free_tot}$ with (B) $k'_6=7.27E-5$, (D) $k'_6=0$, and (F) $k'_6=2.91E-4$. See Table S7 for definitions of $KEAP1_NRF2_{open_tot}$ and $KEAP1_NRF2_{closed_tot}$.

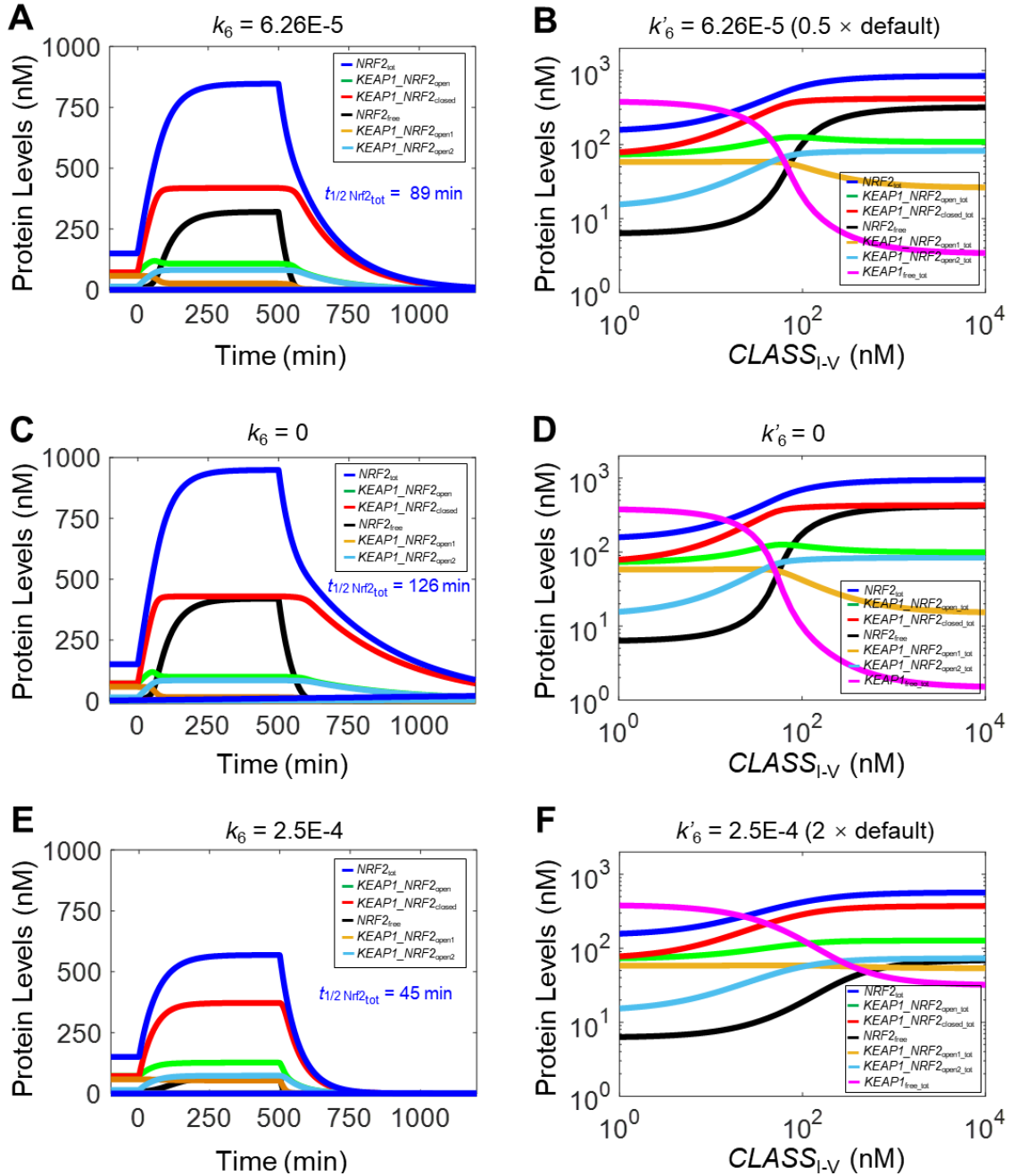


Figure S5. Additional dynamical and steady-state behaviors of Model 3a. Dynamical changes of $NRF2_{free}$, $KEAP1_NRF2_{open1}$, $KEAP1_NRF2_{open2}$, $KEAP1_NRF2_{closed}$, and $NRF2_{tot}$ in response to stabilization of $NRF2$ in $KEAP1_NRF2_{closed}$ by setting (A) $k_6=6.25E-5$, (C) $k_6=0$, and (E) $k_6=2.5E-4$ starting at 0 min and in response to termination of $NRF2$ synthesis (by setting $k_0=0$) starting at 500 min. For simulations in (A, C, and E), $CLASS_{I-V}$ level is kept at zero. Steady-state dose-response curves of various $NRF2$ species and $KEAP1_{free}$ with (B) $k'_6=6.25E-5$, (D) $k'_6=0$, and (F) $k'_6=2.5E-4$. See Table S7 for definitions of $KEAP1_NRF2_{open1_tot}$, $KEAP1_NRF2_{open2_tot}$, and $KEAP1_NRF2_{closed_tot}$.

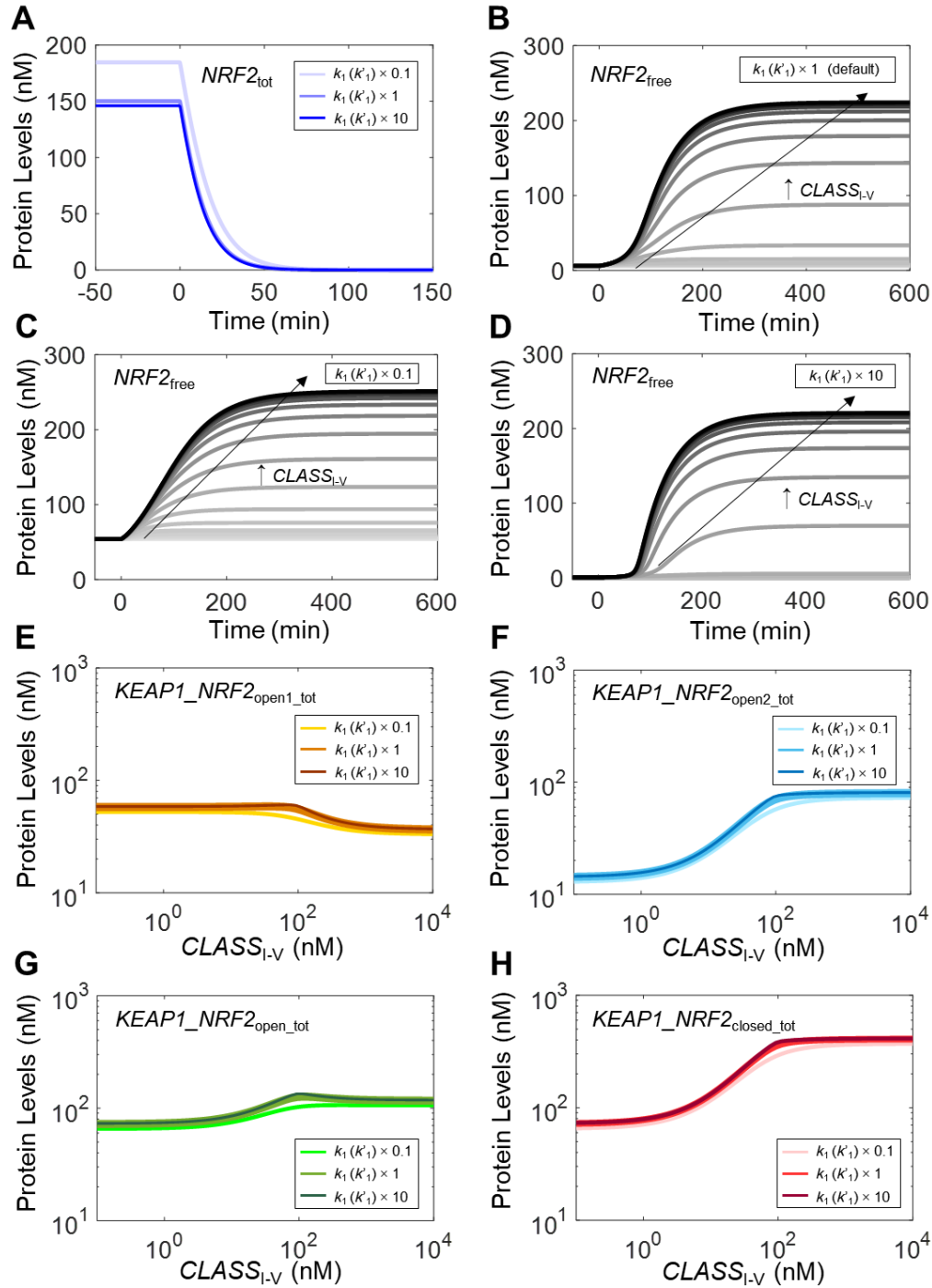
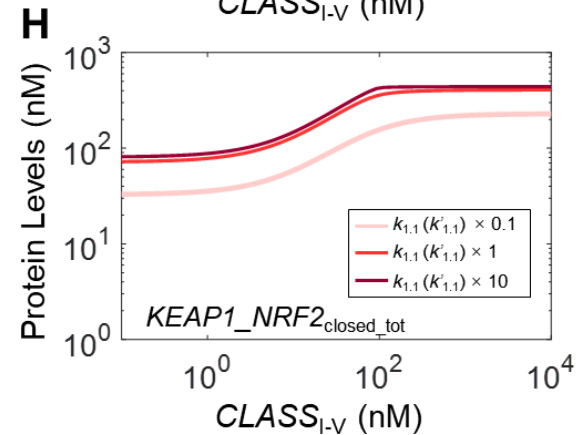
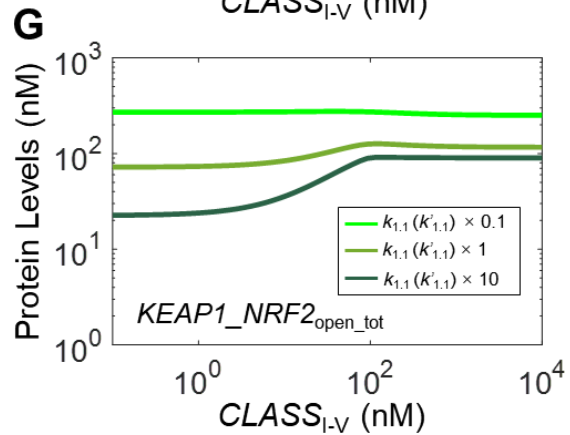
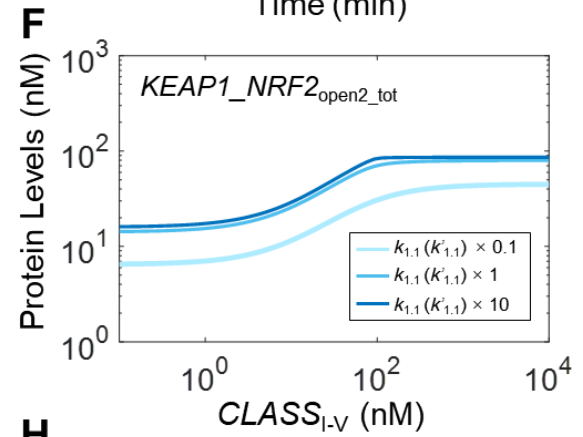
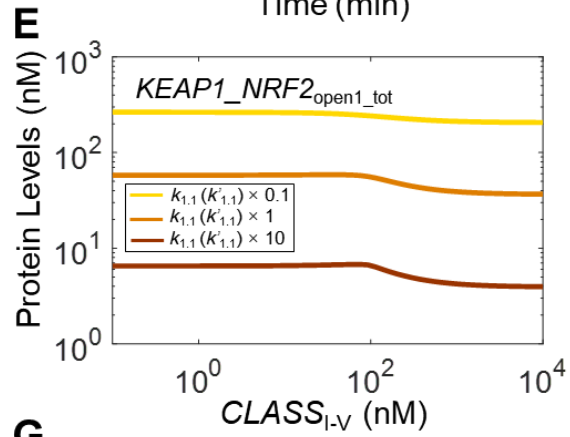
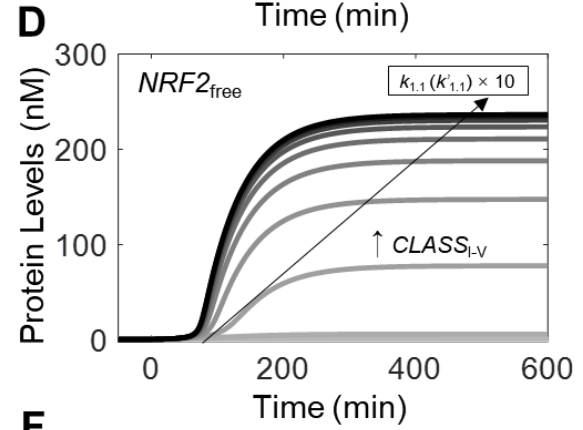
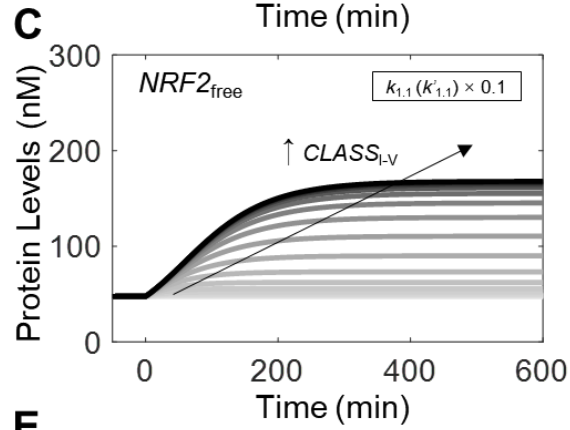
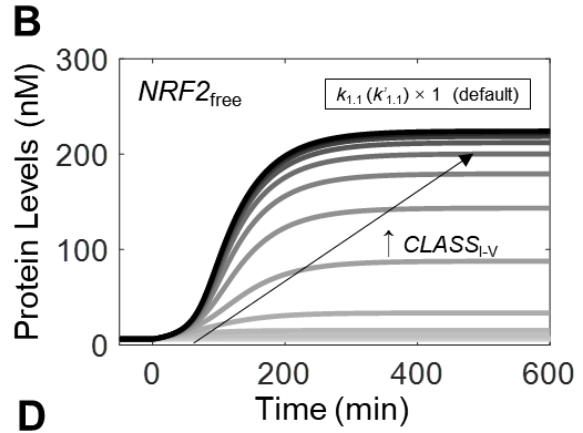
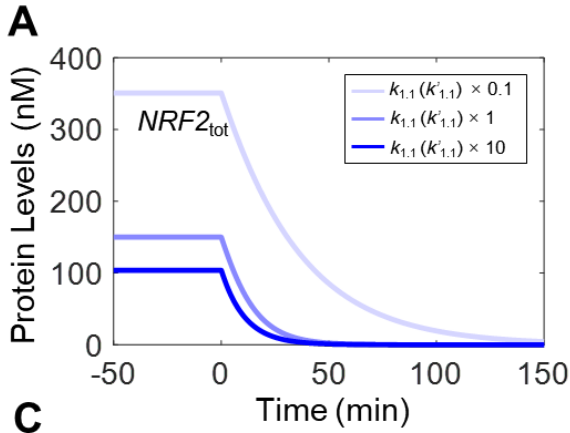


Figure S6. Effects of parameters k_1 (k'_1) on NRF2 responses in Model 3a. (A) Dynamical changes of basal $NRF2_{tot}$ in response to termination of NRF2 synthesis (by setting $k_0=0$) starting at 0 min with $k_1=k'_1$ set at different values from the default. **(B-D)** Dynamical changes of $NRF2_{free}$ in response to different $CLASS_{1-V}$ levels with $k_1=k'_1$ set at different indicated values from the default. **(E-H)** Steady-state dose-response curves of various NRF2 species with $k_1=k'_1$ set at different values from the default.



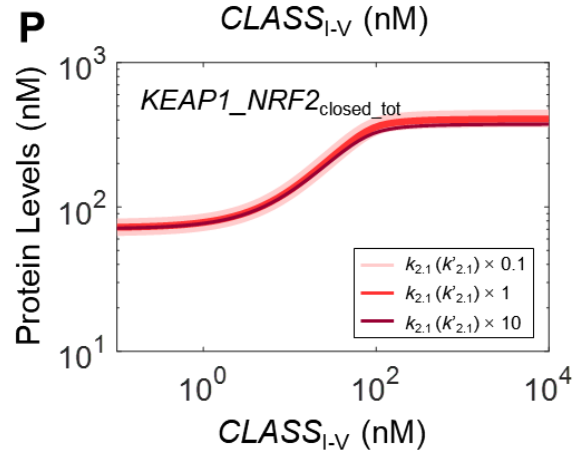
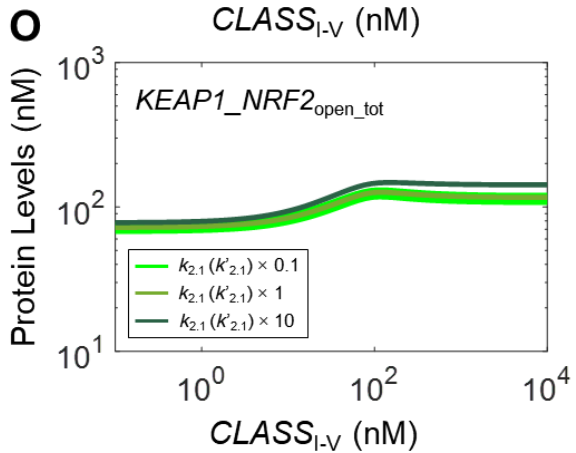
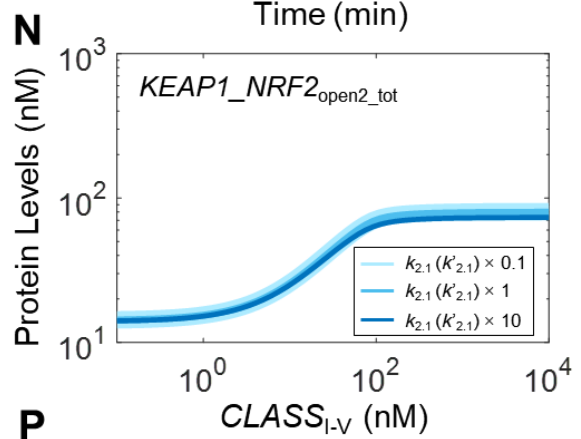
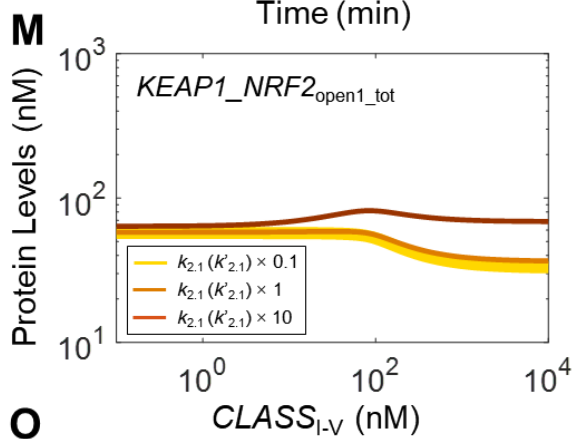
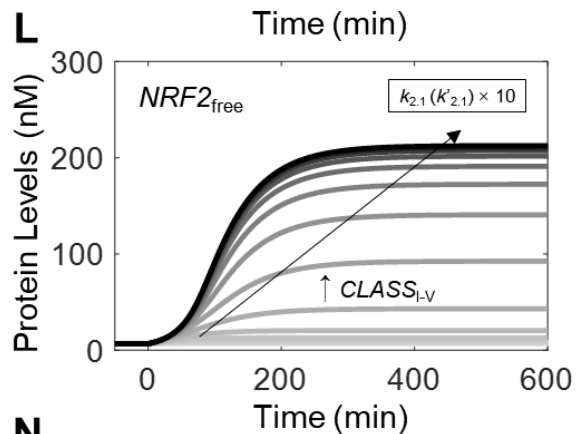
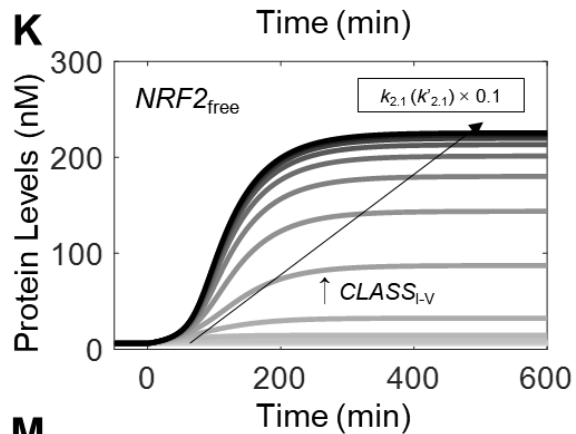
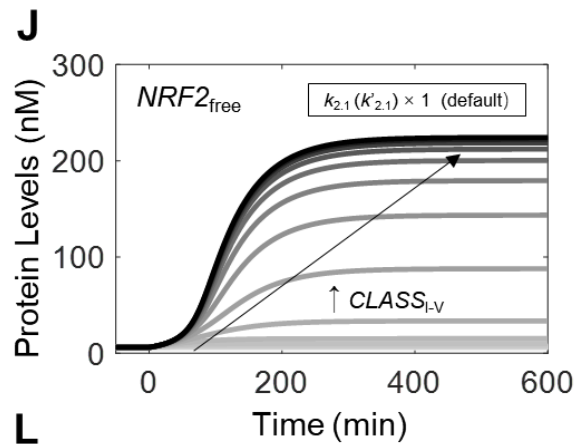
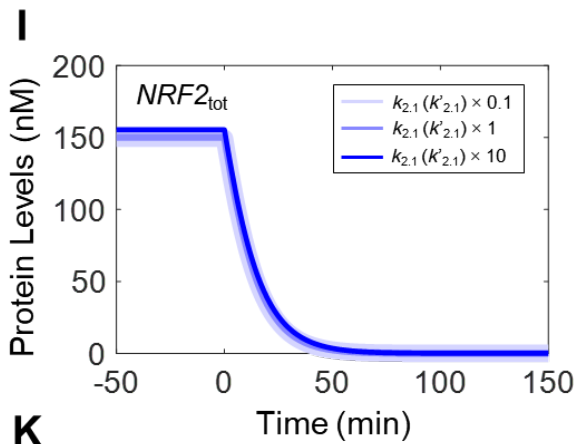


Figure S7. Effects of parameters $k_{1,1}$ ($k'_{1,1}$) and $k_{2,1}$ ($k'_{2,1}$) on NRF2 responses in Model 3a.

(A) Dynamical changes of basal $NRF2_{tot}$ in response to termination of NRF2 synthesis (by setting $k_0=0$) starting at 0 min with $k_{1,1}=k'_{1,1}$ set at different values from the default. **(B-D)** Dynamical changes of $NRF2_{free}$ in response to different $CLASS_{I-V}$ levels with $k_{1,1}=k'_{1,1}$ set at different indicated values from the default. **(E-H)** Steady-state dose-response curves of various NRF2 species with $k_{1,1}=k'_{1,1}$ set at different values from the default. **(I)** Dynamical changes of basal $NRF2_{tot}$ in response to termination of NRF2 synthesis (by setting $k_0=0$) starting at 0 min with $k_{2,1}=k'_{2,1}$ set at different values from the default. **(J-L)** Dynamical changes of $NRF2_{free}$ in response to different $CLASS_{I-V}$ levels with $k_{2,1}=k'_{2,1}$ set at different indicated values from the default. **(M-P)** Steady-state dose-response curves of various NRF2 species with $k_{2,1}=k'_{2,1}$ set at different values from the default.

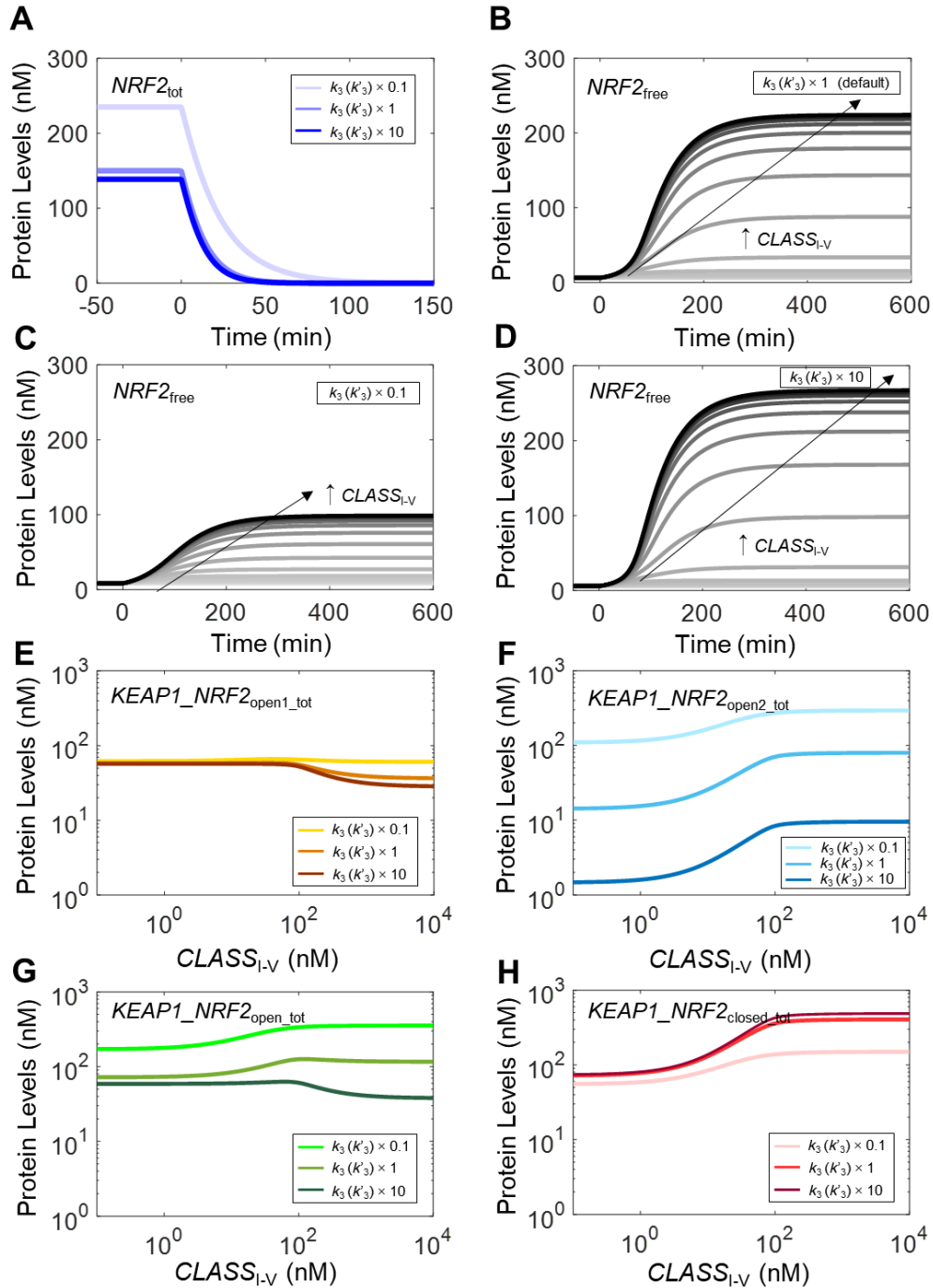


Figure S8. Effects of parameters k_3 (k'_3) on NRF2 responses in Model 3a. (A) Dynamical changes of basal $NRF2_{tot}$ in response to termination of NRF2 synthesis (by setting $k_0=0$) starting at 0 min with $k_3=k'_3$ set at different values from the default. (B-D) Dynamical changes of $NRF2_{free}$ in response to different $CLASS_{1-V}$ levels with $k_3=k'_3$ set at different indicated values from the default. (E-H) Steady-state dose-response curves of various NRF2 species with $k_3=k'_3$ set at different values from the default.

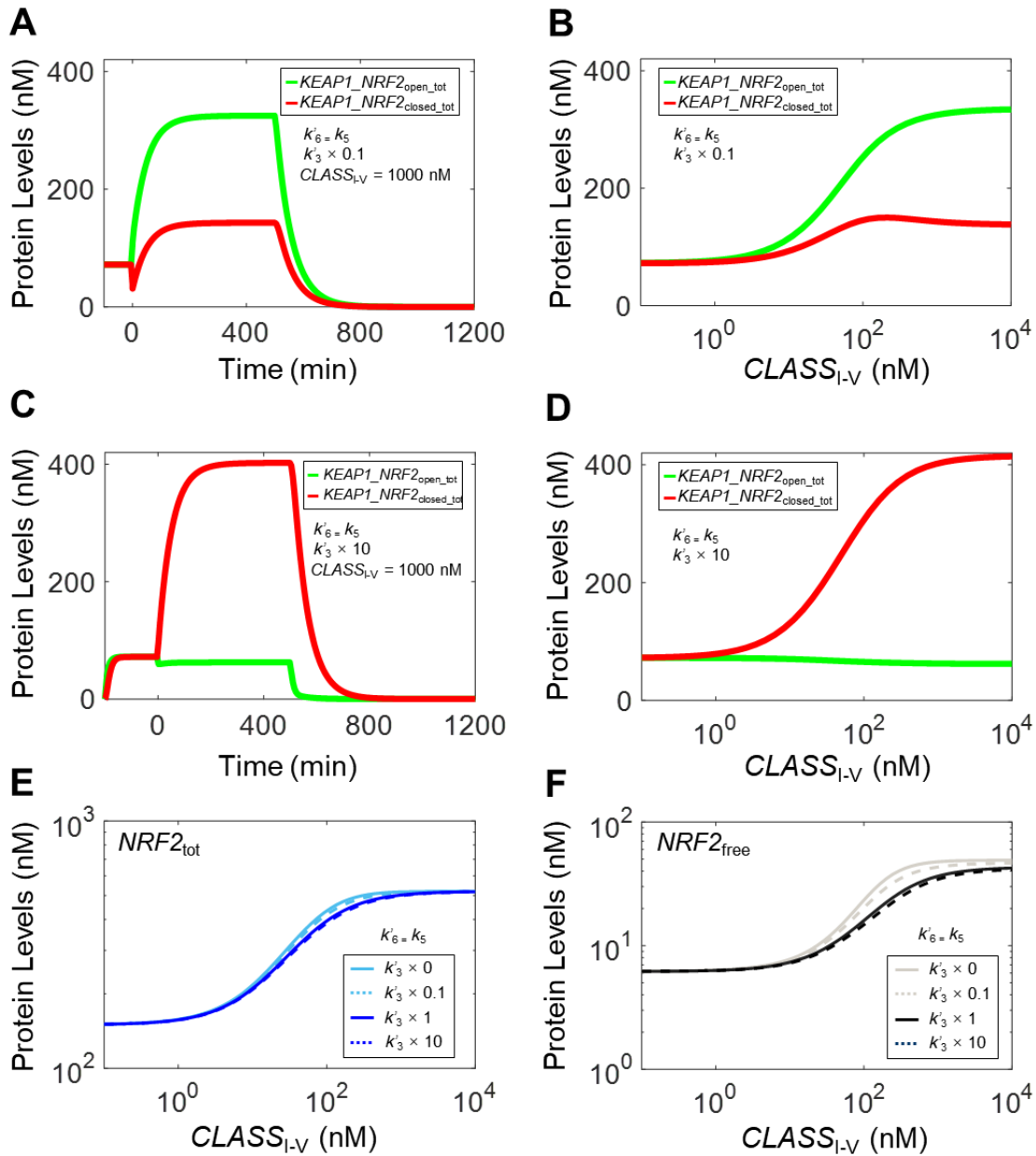


Figure S9. Effects of varying parameter k'_3 alone on NRF2 responses in Model 3a to test hinge-latch hypothesis - with k'_6 set equal to k_5 . Dynamical changes of $KEAP1_NRF2_{open_tot}$ and $KEAP1_NRF2_{closed_tot}$ in response to a high level of $CLASS_{I-V}$ at 1000 nM starting at 0 min and in response to termination of NRF2 synthesis (by setting $k_0=0$) starting at 500 min, when k'_3 is (A) 0.1 and (C) 10 times of default value. Steady-state dose-response curves of $KEAP1_NRF2_{open_tot}$ and $KEAP1_NRF2_{closed_tot}$ when k'_3 is (B) 0.1 and (D) 10 times of default value. (E-F) Effects of varying k'_3 on steady-state dose-response curves of $NRF2_{tot}$ and $NRF2_{free}$ respectively.

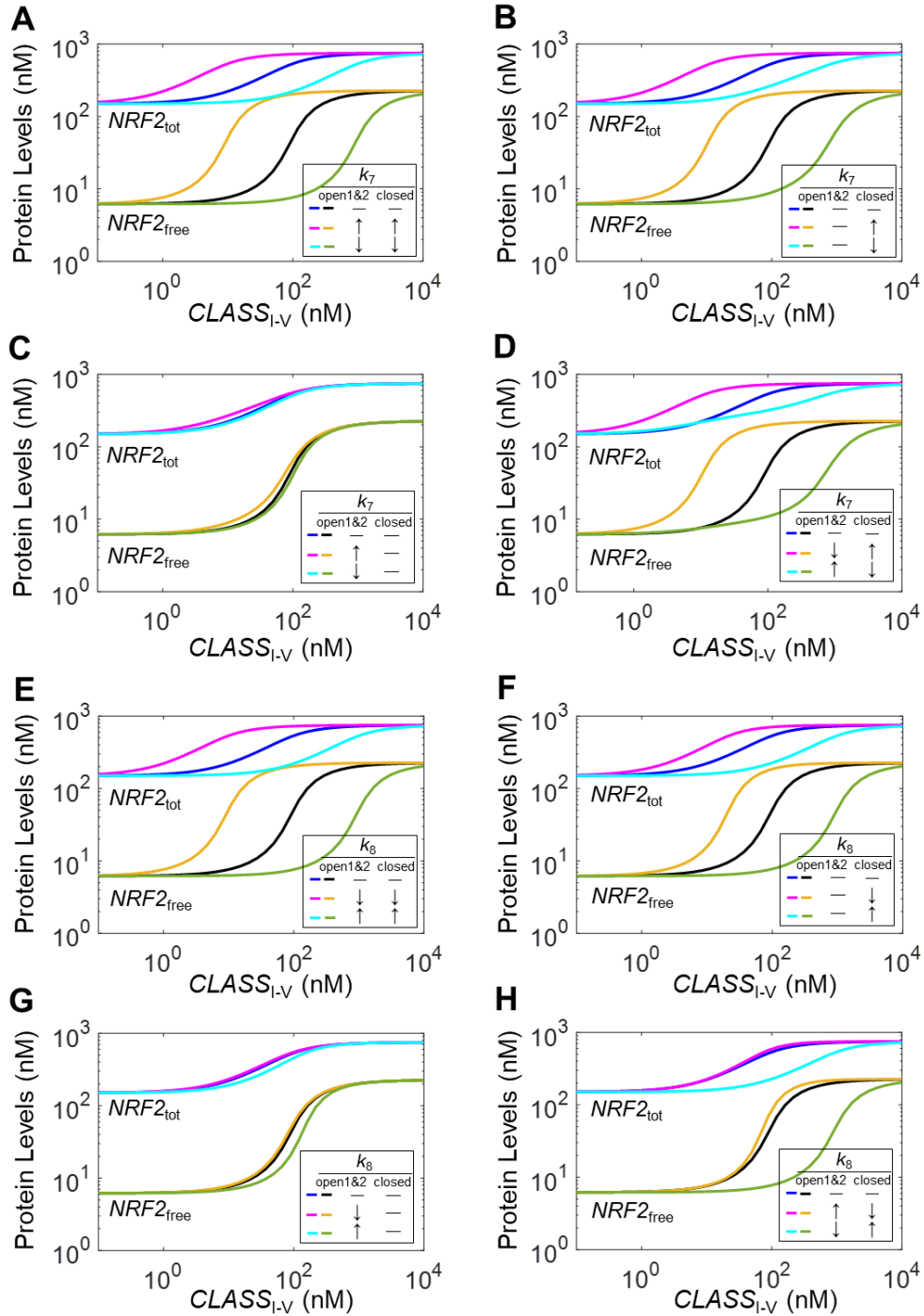


Figure S10. Effects of varying individual parameters k_7 and k_8 for open and closed KEAP1-NRF2 complexes on the steady-state dose-response curves of NRF2 in Model 3a. (A-D) Effects of varying k_7 . (E-H) Effects of varying k_8 . The individual k_7 values for $KEAP1_NRF2_{open1}$ and $KEAP1_NRF2_{open2}$ are varied simultaneously such that they remain equal in all cases, so are the corresponding k_8 values for $KEAP1_NRF2_{open1}$ and $KEAP1_NRF2_{open2}$. Symbols $-$, \uparrow , and \downarrow denote no change, 10X and 0.1X from the default values, respectively.

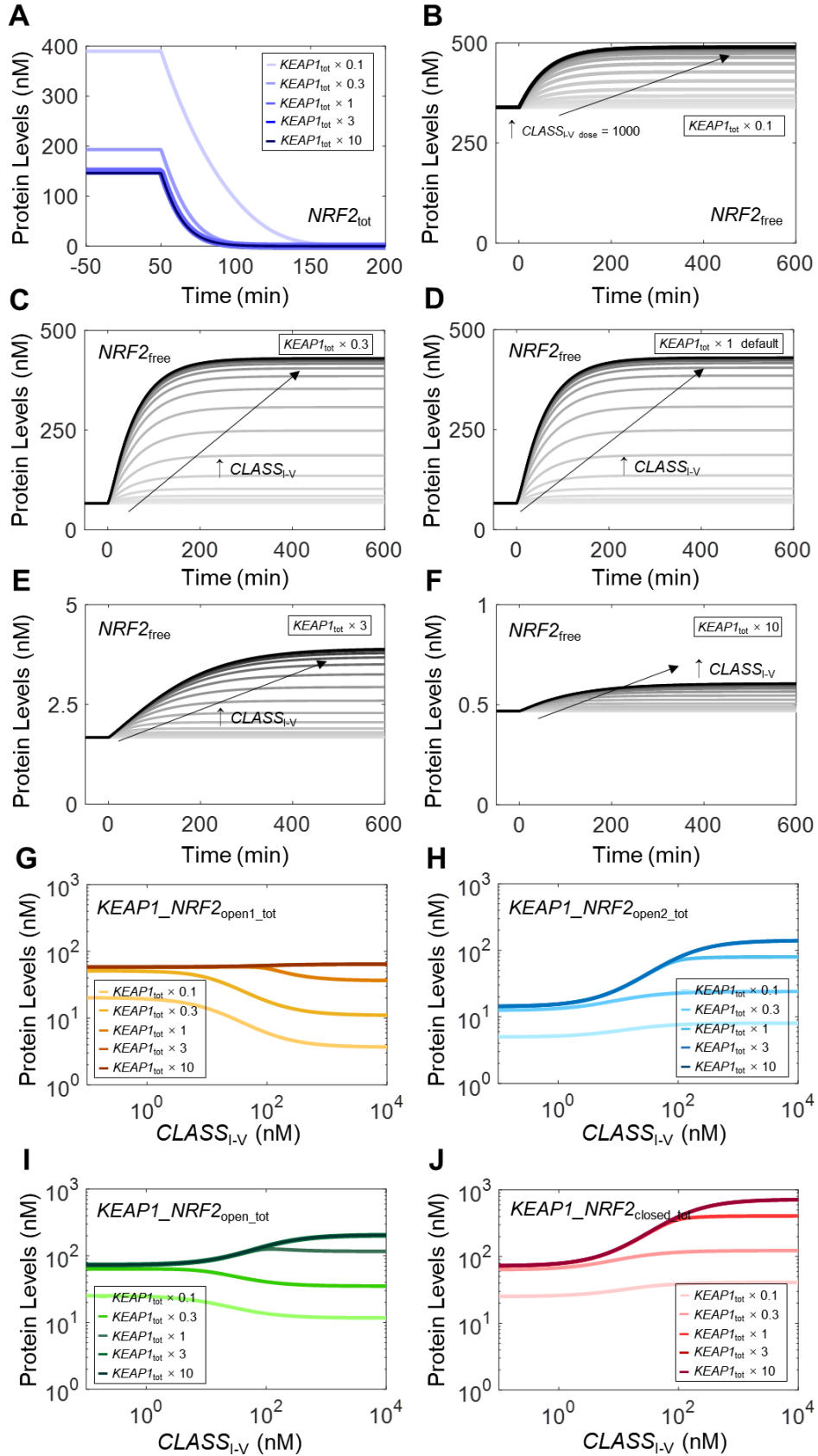


Figure S11. Effects of total KEAP1 abundance on NRF2 responses in Model 3a. (A) Dynamical changes of basal $NRF2_{tot}$ in response to termination of NRF2 synthesis (by setting $k_0=0$) starting at 0 min with $KEAP1_{tot}$ set at different values from the default. **(B-F)** Dynamical changes of $NRF2_{free}$ in response to different $CLASS_{I-V}$ levels with $KEAP1_{tot}$ set at different indicated values from the default. **(G-J)** Steady-state dose-response curves of various Keap1-NRF2 complex species with $KEAP1_{tot}$ set at different values from the default.

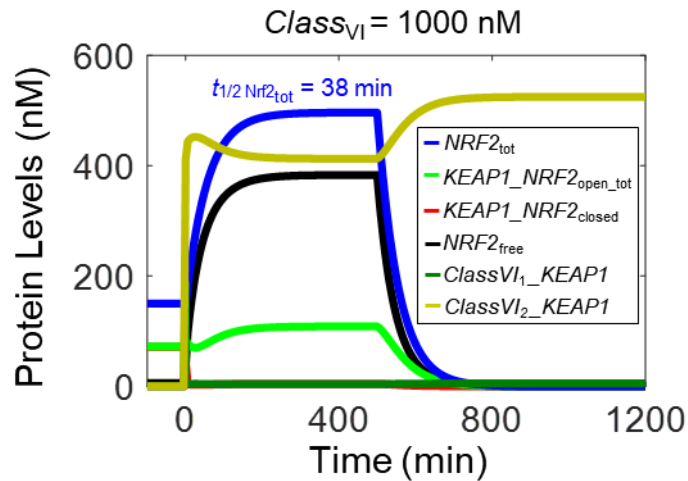


Figure S12. Dynamical changes of various NRF2 species in Model 3b in response to a high $CLASS_{VI}$ level (1000 nM) starting at 0 min and in response to termination of NRF2 synthesis (by setting $k_0=0$) starting at 500 min.

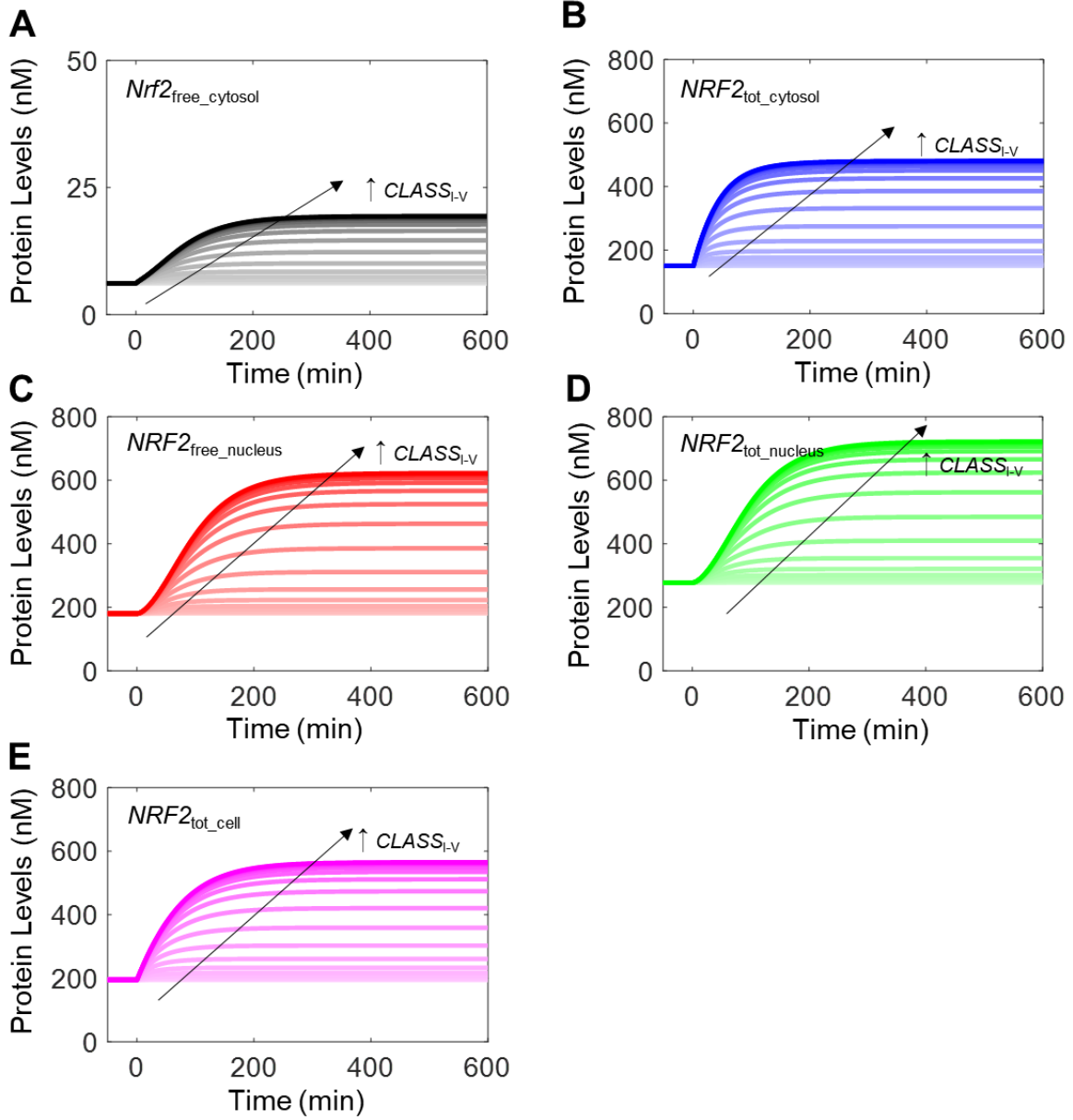


Figure S13. Dynamical changes of various NRF2 species in Model 4a in response to different CLASS_{I-V} levels.

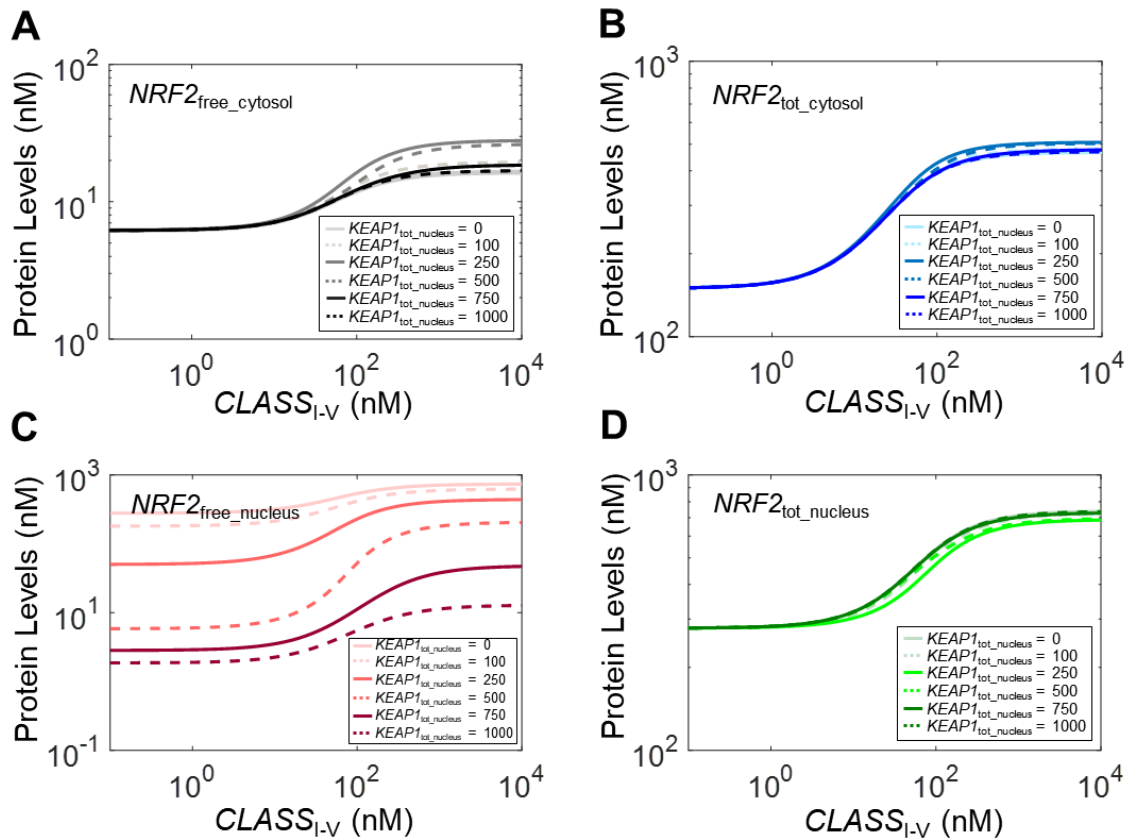


Figure S14. Effects of total nuclear KEAP1 abundance on the steady-state dose-response curves of various NRF2 species in Model 4a. For different total nuclear KEAP1 abundances, k_{10} was adjusted accordingly to (A) 0.02571, (B) 0.01916, (C) 0.01039, (D) 7.405E-3, (E) 7.203E-3, and (F) 7.138E-3, such that the basal steady-state $NRF2_{tot_cytosol}$ and $NRF2_{free_cytosol}$ levels did not deviate from default values.

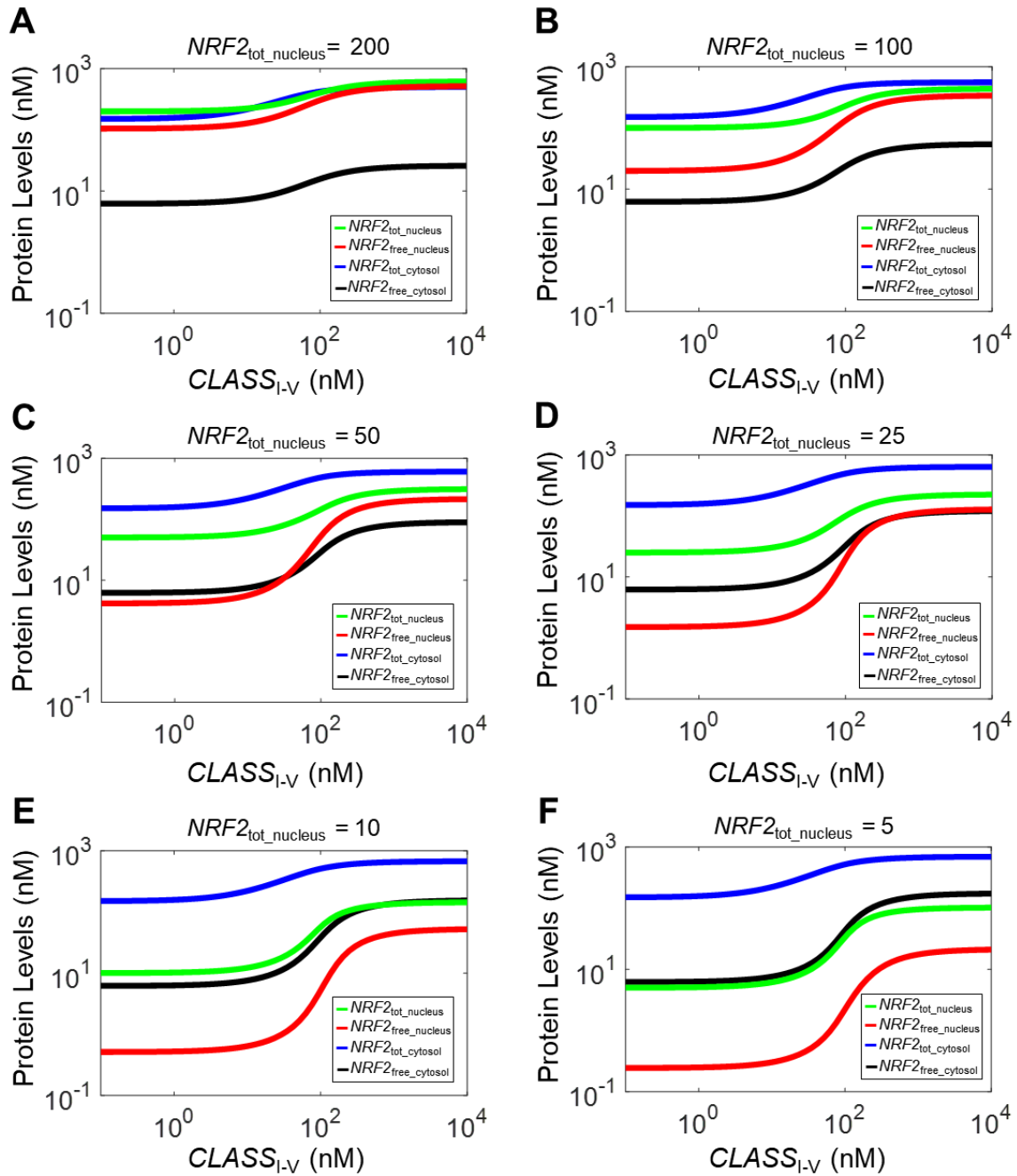
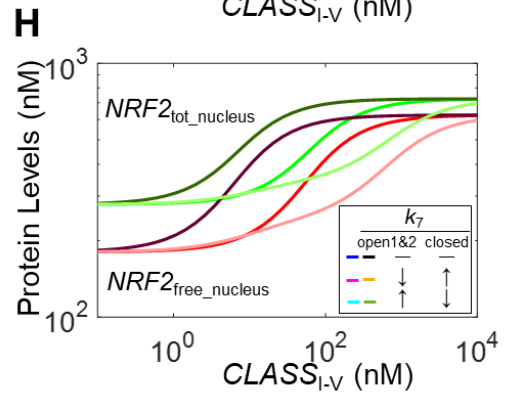
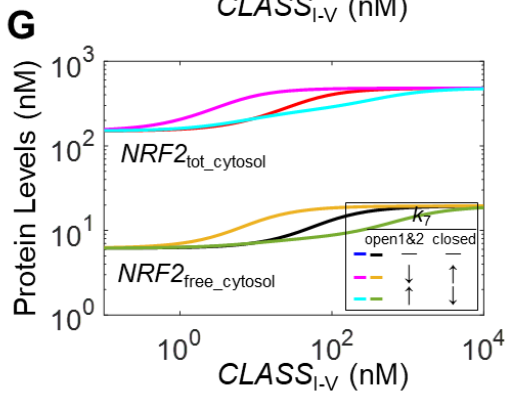
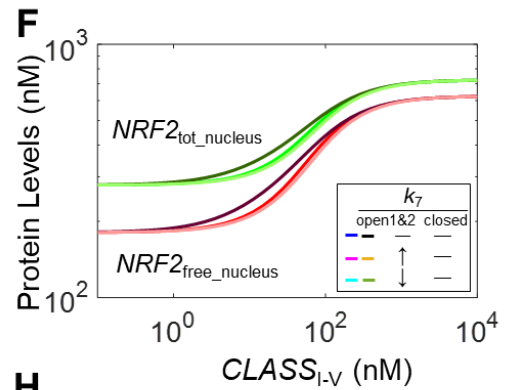
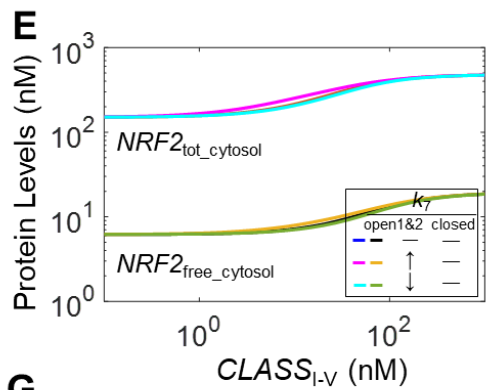
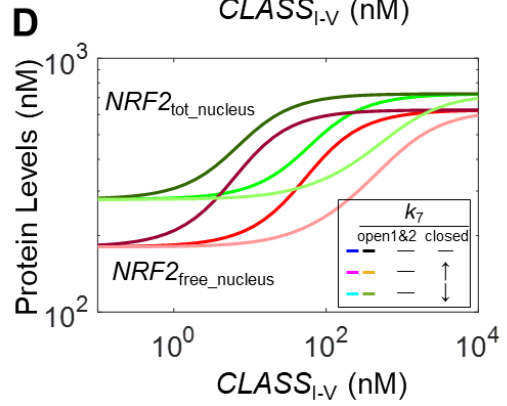
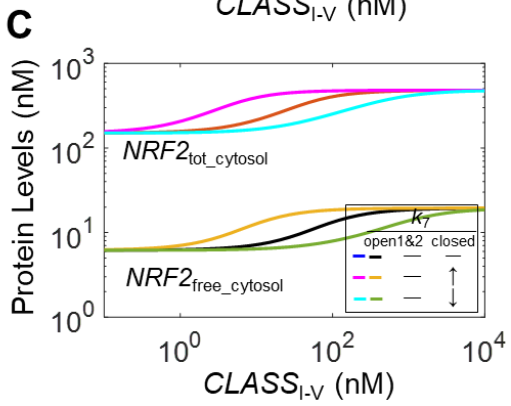
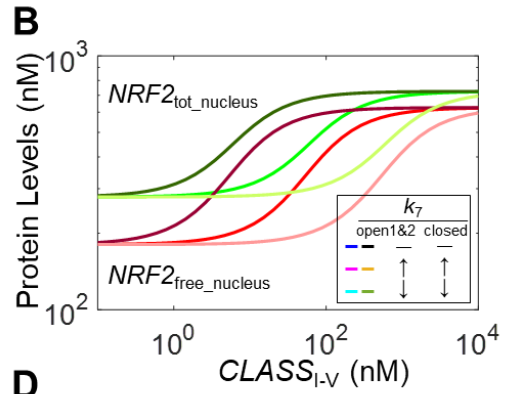
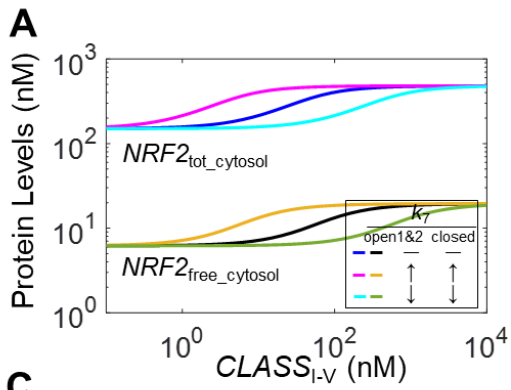


Figure S15. Effects of basal total nuclear NRF2 abundance on steady-state dose-response of various NRF2 species in Model 4a. Different total nuclear NRF2 abundances were achieved by setting (A) $k_0=0.18125$ and $k_{10} = 0.01206$, (B) $k_0=0.16556$ and $k_{10} = 3.849E-3$, (C) $k_0=0.1579$ and $k_{10} = 1.54E-3$, (D) $k_0=0.15398$ and $k_{10} = 7.31E-4$, (E) $k_0=0.1516$ and $k_{10} = 2.87E-4$, and (F) $k_0=0.1509$ and $k_{10} = 1.425E-4$. These pairs of values do not cause deviation of the basal steady-state $NRF2_{tot_cytosol}$ and $NRF2_{free_cytosol}$ levels from default values.



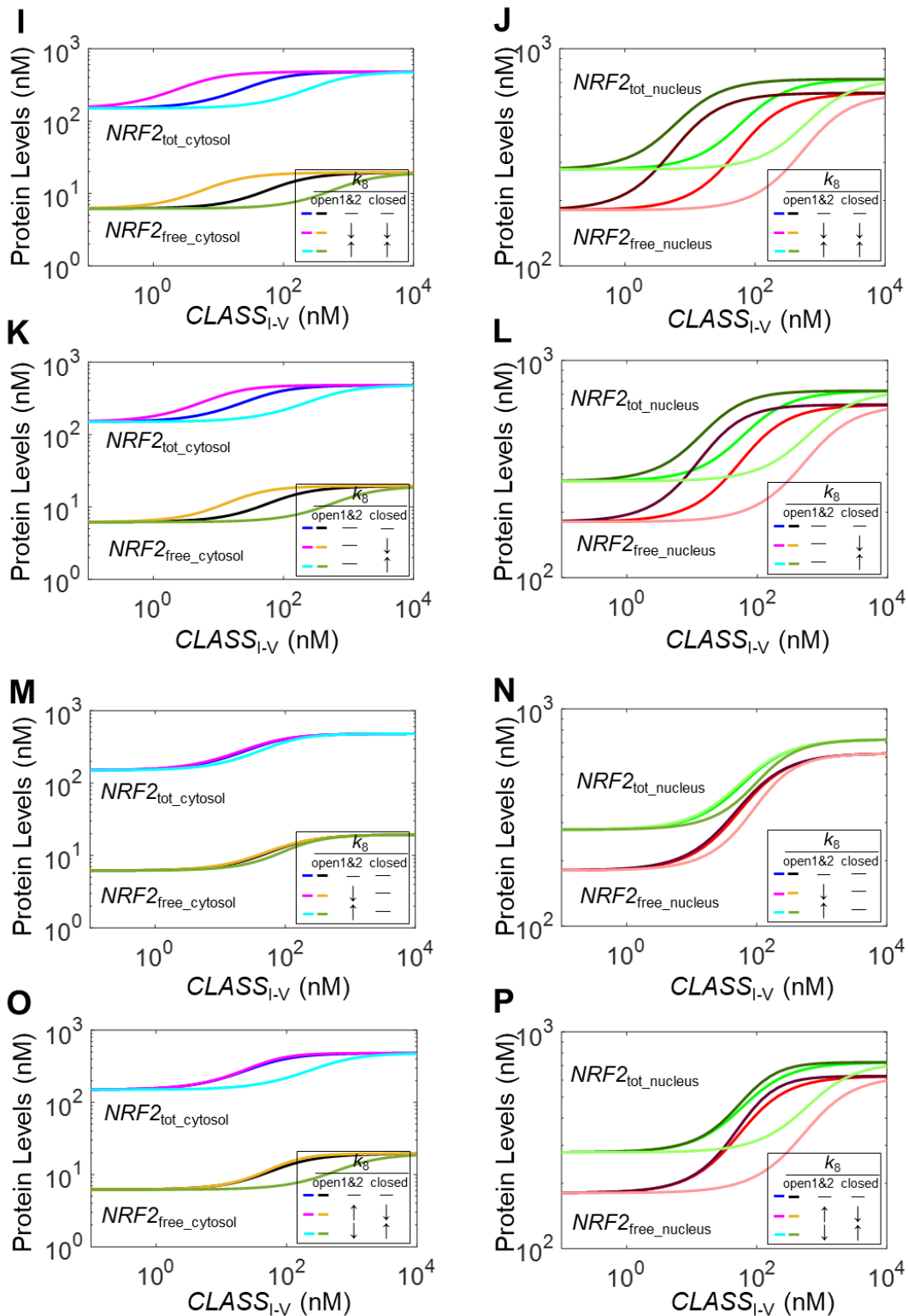


Figure S16. Effects of varying individual parameters k_7 and k_8 for open and closed KEAP1-NRF2 complexes on the steady-state dose-response curves of NRF2 in Model 4a. (A-H) Effects of varying k_7 . (I-P) Effects of varying k_8 . The individual k_7 values for $KEAP1_NRF2_{open1}$ and

$KEAP1_NRF2_{open2}$ are varied simultaneously such that they remain equal in all cases, so are the corresponding k_8 values for $KEAP1_NRF2_{open1}$ and $KEAP1_NRF2_{open2}$. Symbols $-$, \uparrow , and \downarrow denote no change, 10X and 0.1X from the default values, respectively.

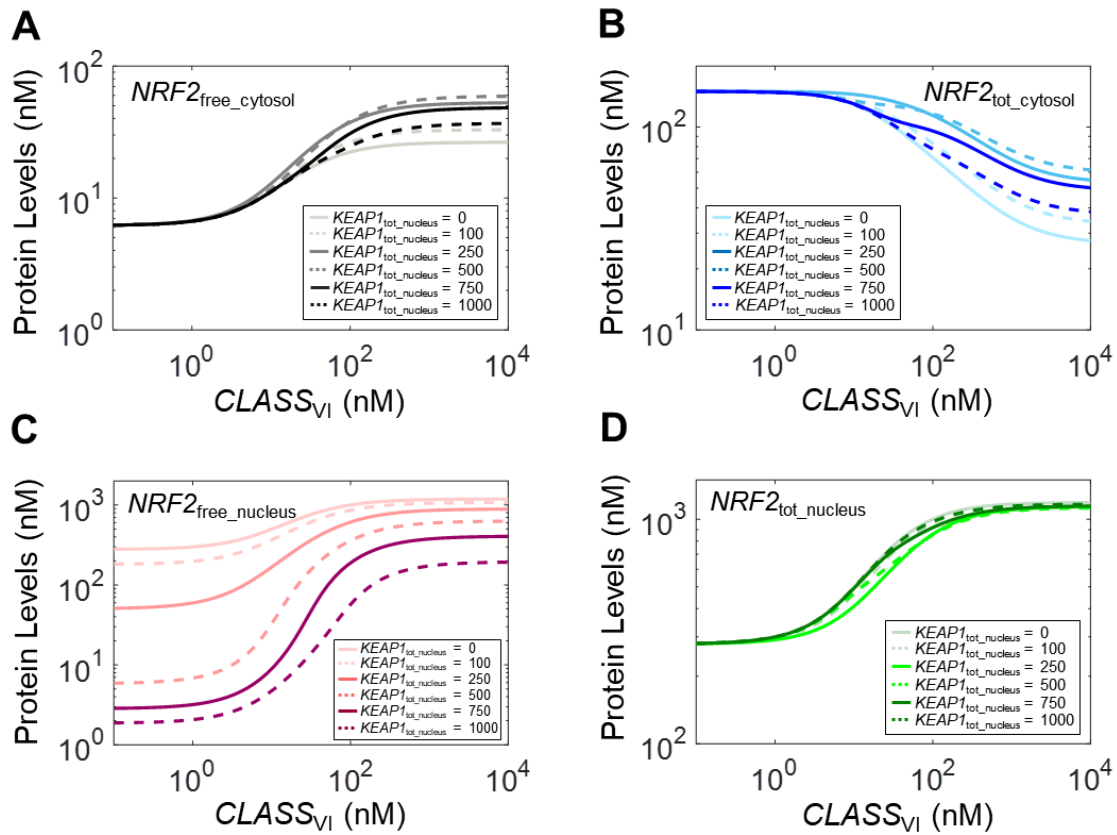


Figure S17. Effects of total nuclear KEAP1 abundance on the steady-state dose-response curves of various NRF2 species in Model 4b. For different total nuclear KEAP1 abundances, k_{10} was adjusted accordingly to values as indicated in Figure S14 legend.

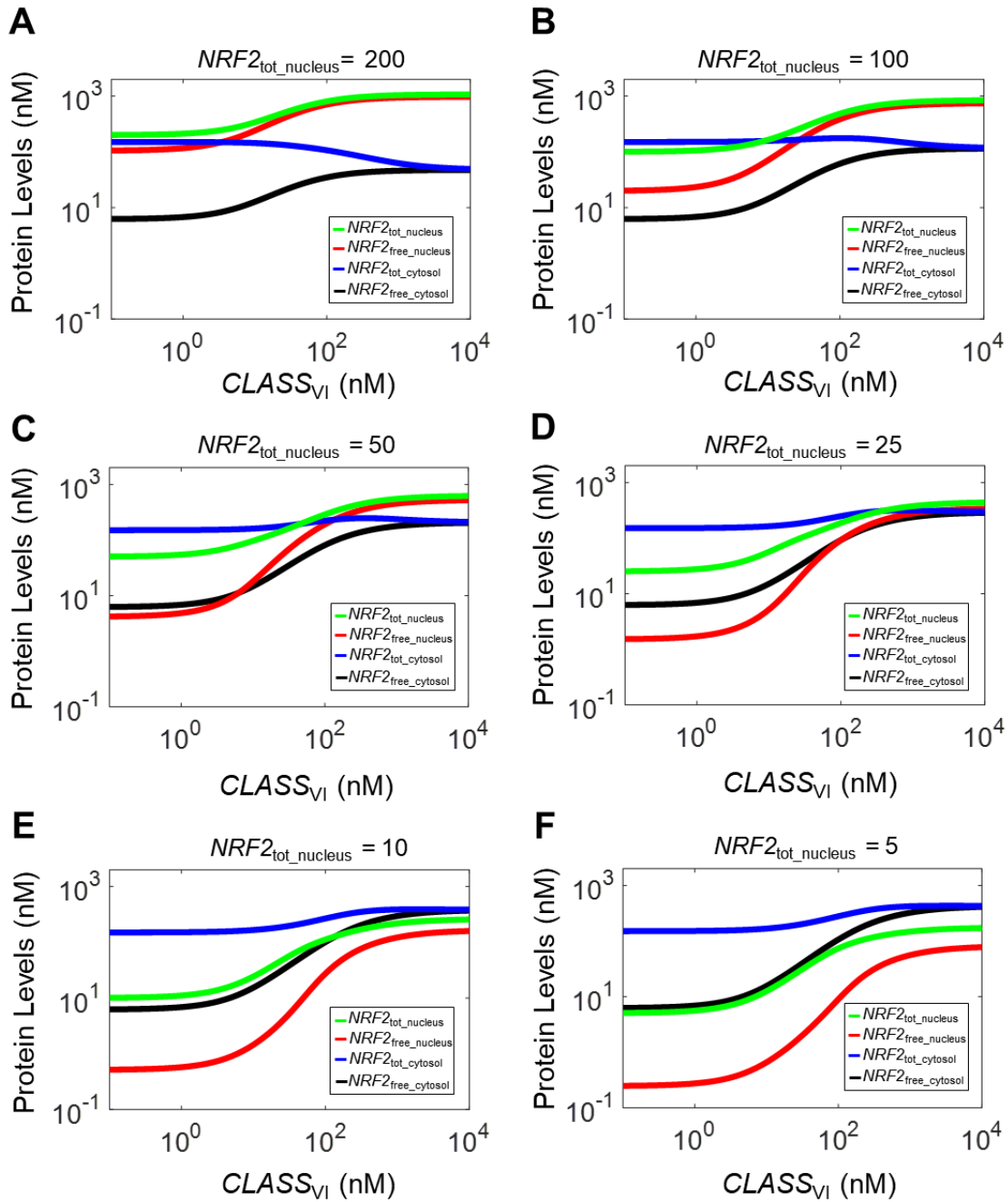


Figure S18. Effects of basal total nuclear NRF2 abundance on steady-state dose-response of various NRF2 species in Model 4b. Different total nuclear NRF2 abundances were achieved with the same k_0 and k_{10} pair settings as in Figure S15 legend.

Tables

Table S1. Model Parameters, Default Values, Sources and Justifications

Parameters	Values						Unit	Note	
	Model 1	Model 2	Model 3a	Model 3b	Model 4a	Model 4b			
k_0	1.721E-1	1.500E-1			1.933E-1		nM/S	i	
k_1, k'_1	1.410E-2		3.450E-3				1/nM/S	ii, xvi	
k_2, k'_2				2.820E-1			1/S	iii, xvi	
$k_{1.1}, k'_{1.1}$	na		2.300E-3				1/S	iv, xvi	
$k_{2.1}, k'_{2.1}$	na		1.220E-4				1/S	v, xvi	
k_3, k'_3	1.975E-1	1.82E-3	1.000	na	1.000	na	1/S	vi, xvi	
k_4, k'_4	1.960E-1	1.000E-4	1.960E-1	na	1.960E-1	na	1/S	vii, xvi	
k_5	2.888E-4						1/S	viii	
k_6	2.03E-3	1.74E-3	1.775E-3				1/S	ix	
k'_6	1.178E-4	1.454E-4	1.252E-4	na	1.252E-4	na	1/S	x	
k_7	1.000E-2						1/nM/S	xi	
k'_7	na			1.000E-2	na	1.000E-2		1/nM/S	xi
k_8	1.000E-1						1/S	xi	
k'_8	na			1.000E-1	na	1.000E-1		1/S	xi
k_9, k'_9	2.888E-4						1/S	xii, xvi	
$k_{9.1}, k'_{9.1}$	na		2.888E-4				1/S	xiii, xvi	
k_{10}	na				1.916E-2		1/S	xiv	
k_{11}	na				7.702E-4		1/S	xv	
k_{n1}	na				3.450E-3		1/nM/S	xvii	
k_{n2}	na				2.820E-1		1/S	xvii	
$k_{n1.1}$	na				2.300E-3		1/S	xvii	
$k_{n2.1}$	na				1.220E-4		1/S	xvii	
k_{n3}	na				1.000		1/S	xvii	
k_{n4}	na				1.960E-1		1/S	xvii	
$k_{n5}, k_{n6}, k_{n9}, k_{n9.1}$	na				2.888E-4		1/S	xvii	
<i>Basal cytosolic total NRF2</i>	150						nM	xviii	
<i>Cytosolic total KEAP1 dimer</i>	530						nM	xix	
<i>Basal total nuclear NRF2</i>	na			278	na	278		nM	xx
<i>Total nuclear KEAP1 dimer</i>	na			100	na	100		nM	xxi
V_n/V_c	na			0.54	na	0.54		-	xxii

na: not applicable

Note:

- (i) k_0 – Zero-order rate constant for *de novo* NRF2 synthesis. As detailed in note *ix*, its value was adjusted iteratively with k_6 to ensure that the cytosolic total NRF2 is 150 nM (note *xviii*) at basal condition.

- (ii) k_1 – Second-order association rate constant for the binding between KEAP1 and the ETGE motif of NRF2. The binding affinities have been reported in several studies with various techniques. Using mouse KEAP1-DC domain fragment and NRF2-Neh2 domain fragment, the association constants (K_a) was reported to be $1.9E8 M^{-1}$ (Tong et al. 2006). Also using mouse KEAP1-DC and NRF2-ETGE peptide, K_a was reported to be $4.42E7 M^{-1}$ (Ichimura et al. 2013) and $3.8E7 M^{-1}$ (Fukutomi et al. 2014). The macroscopic dissociation constants (K_d) between KEAP1-DC and ETGE-containing Neh2 Δ DLGex fragment was 7.31 nM (Fukutomi et al. 2014). The K_d of the binding between a 16-mer peptide containing ETGE and the Kelch domain of KEAP1 was reported to be 20 nM (Lo et al. 2006) and 23.9 nM (Chen et al. 2011). In summary, these values are equivalent to K_d of 5.26, 7.31, 20, 22.62, 23.9, and 26.32 nM. We chose to use $K_d = 20$ nM as default for Models 1 and 2 which involve single-step binding between KEAP1 and ETGE. Therefore, k_1 was calculated as $k_1 = k_2/K_d = 2.82E-1/20 = 1.41E-2 nM^{-1}S^{-1}$.

For Models 3a, 3b, 4a, and 4b, which involve 2-step binding between KEAP1 and ETGE, $3.450E-3 nM^{-1}S^{-1}$ was used for k_1 as reported for the binding between KEAP1-DC and ETGE-containing Neh2 Δ DLGex fragment (Fukutomi et al. 2014).

Given the symmetrical structural configurations of the two monomeric subunits of KEAP1 dimer (Ogura et al. 2010), it is expected that either of the two subunits can equally engage with ETGE. Therefore, the association rate governed by parameter k_1 is multiplied by 2, such that it is $2*k_1*NRF2_{free}*KEAP1_{free}$.

- (iii) k_2 – The dissociation rate constant between KEAP1 and ETGE of NRF2 was determined by using mouse KEAP1-DC fragment and KEAP1-DC and Neh2 Δ DLGex for the first-step binding (Fukutomi et al. 2014).
- (iv) $k_{1.1}$ – The first-order association rate constant for the second-step binding between KEAP1 and ETGE of NRF2 was determined to be $1.2E-3 S^{-1}$ by using mouse KEAP1-DC fragment and KEAP1-DC and Neh2 Δ DLGex (Fukutomi et al. 2014). In our models, this parameter was adjusted to $2.3E-3$, along with k_3 and k_6 to make sure that $KEAP1_NRF2_{open}$ and $KEAP1_NRF2_{closed}$ are equal at basal condition as observed in (Baird et al. 2013).
- (v) $k_{2.1}$ – The first-order dissociation rate constant for the second-step binding between KEAP1 and ETGE of NRF2 was determined by using mouse KEAP1-DC fragment and Neh2 Δ DLGex (Fukutomi et al. 2014).
- (vi) k_3 – The first-order association rate constant between KEAP1 and DLG of NRF2. The binding affinities between KEAP1 and the DLG motif of NRF2 have been reported in a couple of studies. K_a was reported to be $1.0E6 M^{-1}$ between mouse KEAP1-DC domain fragment and NRF2-Neh2 domain fragment (Tong et al. 2006), and $1.9E6 M^{-1}$ between KEAP1-DC and extended DLG motif peptide (DLGex) (Fukutomi et al. 2014). Using mouse KEAP1-DC domain fragment and DLG-containing Neh2(1-56) fragment of NRF2, K_d was reported to be 3.2E3 nM (Fukutomi et al. 2014). In summary, these values are equivalent to K_d of 526, 1000, and 3200 nM.

It is worth noting, however, that the binding between KEAP1-DC and DLG-containing Neh2 fragments in these *in vitro* studies above was measured as intermolecular event. In contrast, because of the much high binding affinity between KEAP1 and ETGE than between KEAP1 and DLG as indicated above, the DLG binding occurs almost always after

ETGE binding between full-length NRF2 and KEAP1 dimer *in vivo*. As a result, the DLG binding is predominantly an intramolecular event. Therefore, k_3 here is actually a first-order association rate constant as opposed to second-order association rate constant measured *in vitro*. For Models 1 and 2, k_3 was determined by manually adjusting its value such that at basal condition, the abundance of open and closed states of KEAP1-NRF2 complex are equal. For Models 3a-4b, k_3 was adjusted, along with $k_{1,1}$, such that basal open:closed ratio is close to 1:1, and when setting $k_0=0$ to observe NRF2 decay, the ratio at 15 min is close to 1:2.5 ratio as in (Baird et al. 2013).

- (vii) k_4 – The dissociation rate constant between KEAP1 and DLG of NRF2 was determined to be $1.960E-1 \text{ S}^{-1}$ by using mouse KEAP1-DC fragment and extended DLG motif peptide (DLGex) (Fukutomi et al. 2014). This value was used in all models except Model 2, in which the value was lowered to $1.0E-4 \text{ S}^{-1}$ to explore the cycle mode of operation for the open and closed KEAP1-NRF2 complexes.
- (viii) k_5 – The first-order rate constant for degradation of free cytosolic NRF2. It was reported that mouse NRF2 is degraded in a KEAP1-independent (redox-independent) manner via the Neh6 domain, with a half-life of about 40 min in COS-1 cells (McMahon et al. 2004) and HEK293T cells (Rada et al. 2011). Therefore, k_5 was determined as $k_5 = \ln(2)/(40*60) = 2.888E-4 \text{ S}^{-1}$.
- (ix) k_6 – First-order rate constant for NRF2 degradation mediated by KEAP1 in the closed state of the KEAP1-NRF2 complex in cytosol at basal condition. NRF2 half-life in whole cell at basal condition has been reported to range mostly between 6-20 min (Kwak et al. 2002, Alam et al. 2003, Itoh et al. 2003, Stewart et al. 2003, Kobayashi et al. 2004, He et al. 2006, Khalil et al. 2015, Crinelli et al. 2021). Since nuclear NRF2 is relatively more stable than cytosolic NRF2 (Itoh et al. 2003, Burroughs et al. 2018), likely mediated by Neh6 involving the GSK-3, β -TrCP, and Cul1 system (Chowdhry et al. 2013), as well as PML-NB (Burroughs et al. 2018), it is reasonable to expect that cytosolic NRF2 is actually degraded at a faster rate than measured in whole cell. We decided to use 10 min as the default cytosolic total NRF2 half-life at basal condition for all models, and k_6 was estimated as follows.
 - a. Since at basal condition, cytosolic KEAP1 dimer is 530 nM and cytosolic total NRF2 is 150 nM (note xviii and xix), given the high binding affinity between KEAP1 and NRF2 mediated by ETGE ($K_d = 20 \text{ nM}$, note ii), the majority of NRF2 is in a KEAP1-NRF2 complex. Therefore, the overall NRF2 half-life at basal condition for Models 1 and 2 can be initially approximated by the rate constants k_9 and k_6 , which govern the degradation of NRF2 in the open and closed states of KEAP1-NRF2 complex, respectively.
 - b. Since the open and closed states of KEAP1-NRF2 complex are in equal abundance (Baird et al. 2013), for an overall NRF2 half-life of 10 min, $\ln(2)/(10*60) = 0.5*k_9+0.5*k_6$, which produced an initial value $k_6=0.002$ (about 5.7-min half-life).
 - c. k_3 in Models 1 and 2 was then adjusted to make sure that open:closed ratio of KEAP1-NRF2 complex = 1:1.
 - d. k_0 was next adjusted to make total NRF2 equal to 150 nM (note xviii) at basal condition.
 - e. k_0 , k_3 and k_6 were fine-tuned iteratively following steps (b)–(d) to make sure that the above 3 conditions (basal total NRF2 half-life = 10 min (by setting $k_0=0$ to observe NRF2 decay), basal total NRF2 = 150 nM, and open:closed ratio = 1:1) are met simultaneously.

- f. As a result of the above adjustments, for Model 1, $k_6=2.03E-3 \text{ S}^{-1}$ (equivalent half-life = 5.7 min); for Model 2, $k_6=1.74E-3 \text{ S}^{-1}$ (equivalent half-life = 6.6 min).
- g. For Model 3a-4b, k_6 was adjusted in a similar spirit, along with additional parameter $k_{1.1}$. The final $k_6=1.775E-3 \text{ S}^{-1}$ (equivalent half-life = 6.5 min).
- (x) k'_6 – First-order rate constant for NRF2 degradation mediated by class I-V compound-oxidized (or conjugated) KEAP1 in the closed state of the KEAP1-NRF2 complex. This is the step where NRF2 stabilization occurs under oxidative stress. k'_6 was estimated to make sure that under full stress cytosolic total NRF2 can increase by 5-fold, which is a reasonable fold-increase (Iso et al. 2016).
- (xi) k_7 (k'_7) and k_8 (k'_8) – For Models 1, 2, 3a and 4a, k_7 is the second-order rate constant for oxidation or conjugation of KEAP1 by class I-V compounds, and k_8 is the first-order rate constant for reduction or deconjugation of KEAP1.

For Models 3b and 4b, k_7 is the second-order association rate constant for the binding between a monomeric subunit of free KEAP1 dimer and class VI compounds, and k_8 is the corresponding first-order dissociation rate constant. Like the k_1 binding step, either of the two KEAP1 subunits in free KEAP1 dimer can equally engage with a class VI compound, thus the association rate governed by parameter k_7 is multiplied by 2, such that it is $2 * k_7 * \text{ClassVI} * \text{KEAP1}_{\text{free}}$.

For Models 3b and 4b, k'_7 is the second-order association rate constant for the binding between the monomeric subunit of KEAP1 dimer already bound by a single class VI compound, and k'_8 is the corresponding first-order dissociation rate constant. We assumed that $k'_7=k_7$ and $k'_8=k_8$.

The values of all these parameters are set so that the oxidation/conjugation or binding events occur fast in the order of seconds. The model behaviors are generally insensitive to these parameters except that varying their values will shift the dose-response curves horizontally.

- (xii) k_9 – First-order rate constant for NRF2 degradation in the open state of KEAP1-NRF2 complex ($\text{KEAP1_NRF2}_{\text{open}}$) for Models 1-2 or the intermediate open state of KEAP1-NRF2 complex ($\text{KEAP1_NRF2}_{\text{open1}}$) for Models 3a-4b in cytosol. Since only in the closed state can KEAP1 mediate the degradation of NRF2, we assume that the degradation of NRF2 in these open states is not affected by ETGE-bound KEAP1 and is equal to the degradation rate constant of free NRF2, such that $k_9=k_5$.
- (xiii) $k_{9.1}$ – First-order rate constant for NRF2 degradation in the final open state of KEAP1-NRF2 complex ($\text{KEAP1_NRF2}_{\text{open2}}$) for Models 3a-4b in cytosol. Since only in the closed state can KEAP1 mediate the degradation of NRF2, we assume that the degradation of NRF2 in this open state is not affected by ETGE-bound KEAP1, such that $k_{9.1}=k_5$.
- (xiv) k_{10} – First-order rate constant for nuclear importation of NRF2 in Models 4a-4b. The value was adjusted along with k_0 such that at basal condition nuclear total NRF2 is 278 nM and cytosolic total NRF2 is 150 nM (note xviii and xx).
- (xv) k_{11} – First-order rate constant for nuclear exportation of free NRF2. The value was set such that it is not rate-limiting and half of nuclear NRF2 can translocate from the nucleus to cytosol

in 15 min (equivalent to average NRF2 nuclear residence time 21.6 min).

- (xvi) k'_i where $i \in \{1, 1.1, 2, 2.1, 3, 4, 9, 9.1\}$ – Parameters for interactions between NRF2 and $KEAP1_o$ (i.e., KEAP1 that is oxidized/conjugated by class I-V compounds or bound by class VI compounds), and parameters for degradation of NRF2 in the open-state complex involving $KEAP1_o$. Since oxidative stress by class I-V compounds do not alter the binding affinity between KEAP1 and NRF2 (Egler et al. 2005, He et al. 2006, Kobayashi et al. 2006, Horie et al. 2021), the k'_i parameters for these binding events were set the same as the corresponding k_i parameters at basal condition where applicable. The degradation rate constants of NRF2 in the open-state complex in these situations are also assumed the same as at basal condition.
- (xvii) k_{ni} where $i \in \{1, 1.1, 2, 2.1, 3, 4, 5, 9, 9.1\}$ – Nuclear parameters corresponding to identically-numbered cytosolic parameters (k_i). Their values were assumed the same as the corresponding cytosolic parameters.
- (xviii) k_{n6} – First-order rate constant for NRF2 degradation in the closed state of the KEAP1-NRF2 complex in nucleus at basal condition. No evidence exists supporting that KEAP1-mediated NRF2 ubiquitination and rapid degradation also occurs in the nucleus, therefore we assumed $k_{n6} = k_{n9}$.
- (xix) **Basal cytosolic total NRF2** – Total cellular NRF2 abundance has been reported to vary greatly among different cell types (Khalil et al. 2015, Iso et al. 2016), however in most of these studies the absolute cytosolic and nuclear NRF2 concentrations were not measured or reported separately. We chose 150 nM as the default value in our model which is the cytosolic total NRF2 concentration reported for RAW 264.7 cells at basal condition (Iso et al. 2016).
- (xx) **Cytosolic total KEAP1 dimer** – Like the case of NRF2, total cellular KEAP1 abundance has been reported to vary greatly among different cell types (Khalil et al. 2015, Iso et al. 2016), however information on the absolute cytosolic and nuclear KEAP1 concentrations is generally lacking. We chose 530 nM as the default value in our model which is the cytosolic total KEAP1 dimer concentration reported for RAW 264.7 cells (Iso et al. 2016). In the Results, we also varied this parameter to explore the effect of KEAP1/NRF2 abundance ratio, which varies greatly among different cell types (Khalil et al. 2015, Iso et al. 2016).
- (xxi) **Basal nuclear total NRF2** – 278 nM was used as the default value in Models 4a and 4b, which is the nuclear total NRF2 concentration reported for RAW 264.7 cells at basal condition (Iso et al. 2016). In the Results, we also varied basal nuclear total NRF2 concentration to explore its effect of on nuclear NRF2 accumulation.
- (xxii) **Nuclear total KEAP1 dimer** – 100 nM was used as the default value in Models 4a and 4b, which is the nuclear total KEAP1 dimer concentration reported for RAW 264.7 cells (Iso et al. 2016). In the Results, we also varied this parameter to explore the effect of nuclear total KEAP1 dimer concentration on nuclear NRF2 accumulation.
- (xxiii) V_n/V_c – Ratio of nuclear volume to cytosolic volume. 0.54 was used in Models 4a and 4b, which is the average ratio for mononuclear cells during mouse embryonic development (Sasaki and Matsumura 1989).

Table S2. ODEs of Models 1 and 2

1	Free NRF2	$\frac{dNRF2_{free}}{dt}$	$= k_0 - k_5 \times NRF2_{free} - 2 \times k_1 \times KEAP1_{free} \times NRF2_{free} + k_2 \times KEAP1_NRF2_{open} - 2 \times k'1 \times KEAP1_{o_free} \times NRF2_{free} + k'2 \times KEAP1_{o_NRF2_{open}}$
2	Free KEAP1 dimer	$\frac{dKEAP1_{free}}{dt}$	$= -2 \times k_1 \times KEAP1_{free} \times NRF2_{free} + k_2 \times KEAP1_NRF2_{open} - k_7 \times KEAP1_{free} \times CLASS_{i-v} + k_8 \times KEAP1_{o_free} + k_6 \times KEAP1_NRF2_{closed} + k_9 \times KEAP1_NRF2_{open}$
3	Free oxidized KEAP1 dimer	$\frac{dKEAP1_{o_free}}{dt}$	$= -2 \times k'1 \times KEAP1_{o_free} \times NRF2_{free} + k'2 \times KEAP1_{o_NRF2_{open}} + k_7 \times KEAP1_{free} \times CLASS_{i-v} - k_8 \times KEAP1_{o_free} + k'9 \times KEAP1_{o_NRF2_{open}} + k'6 \times KEAP1_{o_NRF2_{closed}}$
4	Open-state KEAP1-NRF2 complex	$\frac{dKEAP1_NRF2_{open}}{dt}$	$= 2 \times k_1 \times KEAP1_{free} \times NRF2_{free} - k_2 \times KEAP1_NRF2_{open} - k_3 \times KEAP1_NRF2_{open} + k_4 \times KEAP1_NRF2_{closed} - k_7 \times CLASS_{i-v} \times KEAP1_NRF2_{open} + k_8 \times KEAP1_{o_NRF2_{open}} - k_9 \times KEAP1_NRF2_{open}$
5	Open-state KEAP1 _o -NRF2 complex	$\frac{dKEAP1_{o_NRF2_{open}}}{dt}$	$= 2 \times k'1 \times KEAP1_{o_free} \times NRF2_{free} - k'2 \times KEAP1_{o_NRF2_{open}} - k'3 \times KEAP1_{o_NRF2_{open}} + k'4 \times KEAP1_{o_NRF2_{closed}} + k_7 \times CLASS_{i-v} \times KEAP1_NRF2_{open} - k_8 \times KEAP1_{o_NRF2_{open}} - k'9 \times KEAP1_{o_NRF2_{open}}$
6	Closed-state KEAP1-NRF2 complex	$\frac{dKEAP1_NRF2_{closed}}{dt}$	$= k_3 \times KEAP1_NRF2_{open} - k_4 \times KEAP1_NRF2_{closed} - k_6 \times KEAP1_NRF2_{closed} - k_7 \times CLASS_{i-v} \times KEAP1_NRF2_{closed} + k_8 \times KEAP1_{o_NRF2_{closed}}$
7	Closed-state KEAP1 _o -NRF2 complex	$\frac{dKEAP1_{o_NRF2_{closed}}}{dt}$	$= k'3 \times KEAP1_{o_NRF2_{open}} - k'4 \times KEAP1_{o_NRF2_{closed}} + k_7 \times CLASS_{i-v} \times KEAP1_NRF2_{closed} - k_8 \times KEAP1_{o_NRF2_{closed}} - k'6 \times KEAP1_{o_NRF2_{closed}}$

Table S3. ODEs of Model 3a

1	Free NRF2	$\frac{dNRF2_{free}}{dt}$	=	$k_0 - k_5 \times NRF2_{free} - 2 \times k_1 \times KEAP1_{free} \times NRF2_{free} + k_2 \times KEAP1_NRF2_{open1} - 2 \times k'_{1.1} \times KEAP1_{o_free} \times NRF2_{free} + k'_{2.1} \times KEAP1_{o_NRF2_{open1}}$
2	Free KEAP1 dimer	$\frac{dKEAP1_{free}}{dt}$	=	$- 2 \times k_1 \times KEAP1_{free} \times NRF2_{free} + k_2 \times KEAP1_NRF2_{open1} - k_7 \times KEAP1_{free} \times CLASS_{I-V} + k_8 \times KEAP1_{o_free} + k_6 \times KEAP1_NRF2_{closed} + k_9 \times KEAP1_NRF2_{open1} + k_{9.1} \times KEAP1_NRF2_{open2}$
3	Free oxidized KEAP1 dimer	$\frac{dKEAP1_{o_free}}{dt}$	=	$- 2 \times k'_{1.1} \times KEAP1_{o_free} \times NRF2_{free} + k'_{2.1} \times KEAP1_{o_NRF2_{open1}} + k_7 \times KEAP1_{free} \times CLASS_{I-V} - k_8 \times KEAP1_{o_free} + k'_6 \times KEAP1_{o_NRF2_{closed}} + k'_9 \times KEAP1_{o_NRF2_{open1}} + k'_{9.1} \times KEAP1_{o_NRF2_{open2}}$
4	Intermediate open-state KEAP1-NRF2 complex	$\frac{dKEAP1_NRF2_{open1}}{dt}$	=	$2 \times k_1 \times KEAP1_{free} \times NRF2_{free} - k_2 \times KEAP1_NRF2_{open1} - k_{1.1} \times KEAP1_NRF2_{open1} + k_{2.1} \times KEAP1_NRF2_{open2} - k_7 \times CLASS_{I-V} \times KEAP1_NRF2_{open1} + k_8 \times KEAP1_{o_NRF2_{open1}} - k_9 \times KEAP1_NRF2_{open1}$
5	Intermediate open-state KEAP1 _o -NRF2 complex	$\frac{dKEAP1_{o_NRF2_{open1}}}{dt}$	=	$2 \times k'_{1.1} \times KEAP1_{o_free} \times NRF2_{free} - k'_{2.1} \times KEAP1_{o_NRF2_{open1}} - k'_{1.1} \times KEAP1_{o_NRF2_{open1}} + k'_{2.1} \times KEAP1_{o_NRF2_{open2}} + k_7 \times CLASS_{I-V} \times KEAP1_NRF2_{open1} - k_8 \times KEAP1_{o_NRF2_{open1}} - k'_9 \times KEAP1_{o_NRF2_{open1}}$
6	Final open-state KEAP1-NRF2 complex	$\frac{dKEAP1_NRF2_{open2}}{dt}$	=	$k_{1.1} \times KEAP1_NRF2_{open1} - k_{2.1} \times KEAP1_NRF2_{open2} - k_3 \times KEAP1_NRF2_{open2} + k_4 \times KEAP1_NRF2_{closed} - k_7 \times CLASS_{I-V} \times KEAP1_NRF2_{open2} + k_8 \times KEAP1_{o_NRF2_{open2}} - k_{9.1} \times KEAP1_NRF2_{open2}$
7	Final open-state KEAP1 _o -NRF2 complex	$\frac{dKEAP1_{o_NRF2_{open2}}}{dt}$	=	$k'_{1.1} \times KEAP1_{o_NRF2_{open1}} - k'_{2.1} \times KEAP1_{o_NRF2_{open2}} - k'_3 \times KEAP1_{o_NRF2_{open2}} + k'_4 \times KEAP1_{o_NRF2_{closed}} + k_7 \times CLASS_{I-V} \times KEAP1_NRF2_{open2} - k_8 \times KEAP1_{o_NRF2_{open2}} - k'_{9.1} \times KEAP1_{o_NRF2_{open2}}$
8	Closed-state KEAP1-NRF2 complex	$\frac{dKEAP1_NRF2_{closed}}{dt}$	=	$k_3 \times KEAP1_NRF2_{open2} - k_4 \times KEAP1_NRF2_{closed} - k_6 \times KEAP1_NRF2_{closed} - k_7 \times CLASS_{I-V} \times KEAP1_NRF2_{closed} + k_8 \times KEAP1_{o_NRF2_{closed}}$
9	Closed-state KEAP1 _o -NRF2 complex	$\frac{dKEAP1_{o_NRF2_{closed}}}{dt}$	=	$k'_3 \times KEAP1_{o_NRF2_{open2}} - k'_4 \times KEAP1_{o_NRF2_{closed}} + k_7 \times CLASS_{I-V} \times KEAP1_NRF2_{closed} - k_8 \times KEAP1_{o_NRF2_{closed}} - k'_6 \times KEAP1_{o_NRF2_{closed}}$

Table S4. ODEs of Model 3b

1	Free NRF2	$\frac{dNRF2_{free}}{dt}$	$= k_0 - k_5 \times NRF2_{free} - 2 \times k_1 \times KEAP1_{free} \times NRF2_{free} + k_2 \times KEAP1_NRF2_{open1} - k'_1 \times CLASS_{VI_KEAP1_{free}} \times NRF2_{free} + k'_2 \times CLASS_{VI_KEAP1_NRF2_{open1}}$
2	Free KEAP1 dimer	$\frac{dKEAP1_{free}}{dt}$	$= -2 \times k_1 \times KEAP1_{free} \times NRF2_{free} + k_2 \times KEAP1_NRF2_{open1} - 2 \times k_7 \times KEAP1_{free} \times CLASS_{VI} + k_8 \times CLASS_{VI_KEAP1} + k_6 \times KEAP1_NRF2_{closed} + k_9 \times KEAP1_NRF2_{open1} + k_{9.1} \times KEAP1_NRF2_{open2}$
3	Single ClassVI-bound KEAP1 dimer	$\frac{dCLASS_{VI_KEAP1}}{dt}$	$= -k'_1 \times CLASS_{VI_KEAP1} \times NRF2_{free} + k'_2 \times CLASS_{VI_KEAP1_NRF2_{open1}} + 2 \times k_7 \times KEAP1_{free} \times CLASS_{VI} - k_8 \times CLASS_{VI_KEAP1} - k'_7 \times CLASS_{VI} \times CLASS_{VI_KEAP1} + k'_8 \times CLASS_{VI2_KEAP1} + k'_9 \times CLASS_{VI_KEAP1_NRF2_{open1}} + k'_{9.1} \times CLASS_{VI_KEAP1_NRF2_{open2}}$
4	Dual ClassVI-bound KEAP1 dimer	$\frac{dCLASS_{VI2_KEAP1}}{dt}$	$= k'_7 \times CLASS_{VI} \times CLASS_{VI_KEAP1} - k'_8 \times CLASS_{VI2_KEAP1}$
5	Intermediate open-state KEAP1-NRF2 complex	$\frac{dKEAP1_NRF2_{open1}}{dt}$	$= 2 \times k_1 \times KEAP1_{free} \times NRF2_{free} - k_2 \times KEAP1_NRF2_{open1} - k_{1.1} \times KEAP1_NRF2_{open1} + k_{2.1} \times KEAP1_NRF2_{open2} - k_7 \times CLASS_{VI} \times KEAP1_NRF2_{open1} + k_8 \times CLASS_{VI_KEAP1_NRF2_{open1}} - k_9 \times KEAP1_NRF2_{open1}$
6	Final open-state KEAP1-NRF2 complex	$\frac{dKEAP1_NRF2_{open2}}{dt}$	$= k_{1.1} \times KEAP1_NRF2_{open1} - k_{2.1} \times KEAP1_NRF2_{open2} - k_3 \times KEAP1_NRF2_{open2} + k_4 \times KEAP1_NRF2_{closed} - k_7 \times CLASS_{VI} \times KEAP1_NRF2_{open2} + k_8 \times CLASS_{VI_KEAP1_NRF2_{open2}} - k_{9.1} \times KEAP1_NRF2_{open2}$
7	Closed-state KEAP1-NRF2 complex	$\frac{dKEAP1_NRF2_{closed}}{dt}$	$= k_3 \times KEAP1_NRF2_{open2} - k_4 \times KEAP1_NRF2_{closed} - k_6 \times KEAP1_NRF2_{closed}$
8	Intermediate open-state ClassVI-KEAP1-NRF2 complex	$\frac{dCLASS_{VI_KEAP1_NRF2_{open1}}}{dt}$	$= k'_1 \times CLASS_{VI_KEAP1} \times NRF2_{free} - k'_2 \times CLASS_{VI_KEAP1_NRF2_{open1}} - k'_{1.1} \times CLASS_{VI_KEAP1_NRF2_{open1}} + k'_{2.1} \times CLASS_{VI_KEAP1_NRF2_{open2}} + k_7 \times CLASS_{VI} \times KEAP1_NRF2_{open1} - k_8 \times CLASS_{VI_KEAP1_NRF2_{open1}} - k'_9 \times CLASS_{VI_KEAP1_NRF2_{open1}}$
9	Final open-state ClassVI-KEAP1-NRF2 complex	$\frac{dCLASS_{VI_KEAP1_NRF2_{open2}}}{dt}$	$= k'_{1.1} \times CLASS_{VI_KEAP1_NRF2_{open1}} - k'_{2.1} \times CLASS_{VI_KEAP1_NRF2_{open2}} + k_7 \times CLASS_{VI} \times KEAP1_NRF2_{open2} - k_8 \times CLASS_{VI_KEAP1_NRF2_{open2}} - k'_{9.1} \times CLASS_{VI_KEAP1_NRF2_{open2}}$

Table S5. ODEs of Model 4a

1	Cytosolic free NRF2	$\frac{dNRF2_{free_cytosol}}{dt}$	$= k_0 - k_5 \times NRF2_{free_cytosol} - 2 \times k_1 \times KEAP1_{free_cytosol} \times NRF2_{free_cytosol} + k_2 \times KEAP1_NRF2_{open1_cytosol}$ $- 2 \times k'_1 \times KEAP1_{o_free_cytosol} \times NRF2_{free_cytosol} + k'_2 \times KEAP1_{o_NRF2_{open1_cytosol}} - k_{10} \times NRF2_{free_cytosol}$ $+ k_{11} \times NRF2_{free_nucleus} \times \frac{V_n}{V_c}$
2	Cytosolic free KEAP1 dimer	$\frac{dKEAP1_{free_cytosol}}{dt}$	$= - 2 \times k_1 \times KEAP1_{free_cytosol} \times NRF2_{free_cytosol} + k_2 \times KEAP1_NRF2_{open1_cytosol} - k_7 \times KEAP1_{free_cytosol} \times CLASS_{i-v}$ $+ k_8 \times KEAP1_{o_free_cytosol} + k_6 \times KEAP1_NRF2_{closed_cytosol} + k_9 \times KEAP1_NRF2_{open1_cytosol}$ $+ k_{9.1} \times KEAP1_NRF2_{open2_cytosol}$
3	Cytosolic free oxidized KEAP1 dimer	$\frac{dKEAP1_{o_free_cytosol}}{dt}$	$= - 2 \times k'_1 \times KEAP1_{o_free_cytosol} \times NRF2_{free_cytosol} + k'_2 \times KEAP1_{o_NRF2_{open1_cytosol}} + k_7 \times KEAP1_{free_cytosol} \times CLASS_{i-v}$ $- k_8 \times KEAP1_{o_free_cytosol} + k'_6 \times KEAP1_{o_NRF2_{closed_cytosol}} + k'_9 \times KEAP1_{o_NRF2_{open1_cytosol}}$ $+ k'_{9.1} \times KEAP1_{o_NRF2_{open2_cytosol}}$
4	Cytosolic intermediate open-state KEAP1-NRF2 complex	$\frac{dKEAP1_NRF2_{open1_cytosol}}{dt}$	$= 2 \times k_1 \times KEAP1_{free_cytosol} \times NRF2_{free_cytosol} - k_2 \times KEAP1_NRF2_{open1_cytosol} - k_{1.1} \times KEAP1_NRF2_{open1_cytosol}$ $+ k_{2.1} \times KEAP1_NRF2_{open2_cytosol} - k_7 \times CLASS_{i-v} \times KEAP1_NRF2_{open1_cytosol}$ $+ k_8 \times KEAP1_{o_NRF2_{open1_cytosol}} - k_9 \times KEAP1_NRF2_{open1_cytosol}$
5	Cytosolic intermediate open-state KEAP1 _o -NRF2 complex	$\frac{dKEAP1_{o_NRF2_{open1_cytosol}}}{dt}$	$= 2 \times k'_1 \times KEAP1_{o_free_cytosol} \times NRF2_{free_cytosol} - k'_2 \times KEAP1_{o_NRF2_{open1_cytosol}} - k'_{1.1} \times KEAP1_{o_NRF2_{open1_cytosol}}$ $+ k'_{2.1} \times KEAP1_{o_NRF2_{open2_cytosol}} + k_7 \times CLASS_{i-v} \times KEAP1_{o_NRF2_{open1_cytosol}} - k_8 \times KEAP1_{o_NRF2_{open1_cytosol}}$ $- k'_9 \times KEAP1_{o_NRF2_{open1_cytosol}}$
6	Cytosolic final open-state KEAP1-NRF2 complex	$\frac{dKEAP1_NRF2_{open2_cytosol}}{dt}$	$= k_{1.1} \times KEAP1_NRF2_{open1_cytosol} - k_{2.1} \times KEAP1_NRF2_{open2_cytosol} - k_3 \times KEAP1_NRF2_{open2_cytosol}$ $+ k_4 \times KEAP1_NRF2_{closed_cytosol} - k_7 \times CLASS_{i-v} \times KEAP1_NRF2_{open2_cytosol} + k_8 \times KEAP1_{o_NRF2_{open2_cytosol}}$ $- k_{9.1} \times KEAP1_NRF2_{open2_cytosol}$
7	Cytosolic final open-state KEAP1 _o -NRF2 complex	$\frac{dKEAP1_{o_NRF2_{open2_cytosol}}}{dt}$	$= k'_{1.1} \times KEAP1_{o_NRF2_{open1_cytosol}} - k'_{2.1} \times KEAP1_{o_NRF2_{open2_cytosol}} - k'_3 \times KEAP1_{o_NRF2_{open2_cytosol}}$ $+ k'_{4} \times KEAP1_{o_NRF2_{closed_cytosol}} + k_7 \times CLASS_{i-v} \times KEAP1_{o_NRF2_{open2_cytosol}} - k_8 \times KEAP1_{o_NRF2_{open2_cytosol}}$ $- k'_{9.1} \times KEAP1_{o_NRF2_{open2_cytosol}}$
8	Cytosolic closed-state KEAP1-NRF2 complex	$\frac{dKEAP1_NRF2_{closed_cytosol}}{dt}$	$= k_3 \times KEAP1_NRF2_{open2_cytosol} - k_4 \times KEAP1_NRF2_{closed_cytosol} - k_6 \times KEAP1_NRF2_{closed_cytosol}$ $- k_7 \times CLASS_{i-v} \times KEAP1_NRF2_{closed_cytosol} + k_8 \times KEAP1_{o_NRF2_{closed_cytosol}}$
9	Cytosolic closed-state KEAP1 _o -NRF2 complex	$\frac{dKEAP1_{o_NRF2_{closed_cytosol}}}{dt}$	$= k'_3 \times KEAP1_{o_NRF2_{open2_cytosol}} - k'_4 \times KEAP1_{o_NRF2_{closed_cytosol}} + k_7 \times CLASS_{i-v} \times KEAP1_{o_NRF2_{closed_cytosol}}$ $- k_8 \times KEAP1_{o_NRF2_{closed_cytosol}} - k'_6 \times KEAP1_{o_NRF2_{closed_cytosol}}$
10	Nuclear free NRF2	$\frac{dNRF2_{free_nucleus}}{dt}$	$= k_{10} \times NRF2_{free_cytosol} \times \frac{V_c}{V_n} - k_{11} \times NRF2_{free_nucleus} - k_{n5} \times NRF2_{free_nucleus} - 2 \times k_{n1} \times NRF2_{free_nucleus} \times KEAP1_{free_nucleus}$ $+ k_{n2} \times KEAP1_NRF2_{open1_nucleus}$
11	Nuclear free KEAP1	$\frac{dKEAP1_{free_nucleus}}{dt}$	$= - 2 \times k_{n1} \times NRF2_{free_nucleus} \times KEAP1_{free_nucleus} + k_{n2} \times KEAP1_NRF2_{open1_nucleus} + k_{n6} \times KEAP1_NRF2_{closed_nucleus}$ $+ k_{n9} \times KEAP1_NRF2_{open1_nucleus} + k_{n9.1} \times KEAP1_NRF2_{open2_nucleus}$

12	Nuclear intermediate open-state KEAP1-NRF2 complex	$\frac{dKEAP1_NRF2_{open1_nucleus}}{dt} = 2 \times k_{n1} \times NRF2_{free_nucleus} \times KEAP1_{free_nucleus} - k_{n2} \times KEAP1_NRF2_{open1_nucleus} - k_{n1.1} \times KEAP1_NRF2_{open1_nucleus} + k_{n2.1} \times KEAP1_NRF2_{open2_nucleus} - k_{n9} \times KEAP1_NRF2_{open1_nucleus}$
----	--	---

13	Nuclear final open-state KEAP1-NRF2 complex	$\frac{dKEAP1_NRF2_{open2_nucleus}}{dt} = k_{n1.1} \times KEAP1_NRF2_{open1_nucleus} - k_{n2.1} \times KEAP1_NRF2_{open2_nucleus} - k_{n3} \times KEAP1_NRF2_{open2_nucleus} + k_{n4} \times KEAP1_NRF2_{closed_nucleus} - k_{n9.1} \times KEAP1_NRF2_{open2_nucleus}$
----	---	--

14	Nuclear closed-state KEAP1-NRF2 complex	$\frac{dKEAP1_NRF2_{closed_nucleus}}{dt} = k_{n3} \times KEAP1_NRF2_{open2_nucleus} - k_{n4} \times KEAP1_NRF2_{closed_nucleus} - k_{n6} \times KEAP1_NRF2_{closed_nucleus}$
----	---	--

Table S6. ODEs of Model 4b

1	Cytosolic free NRF2	$\frac{dNRF2_{free_cytosol}}{dt}$	=	$k_0 - k_5 \times NRF2_{free_cytosol} - 2 \times k_1 \times KEAP1_{free_cytosol} \times NRF2_{free_cytosol} + k_2 \times KEAP1_NRF2_{open1_cytosol}$ $- k'_1 \times CLASS_{VI_KEAP1}_{free_cytosol} \times NRF2_{free_cytosol} + k'_2 \times CLASS_{VI_KEAP1_NRF2}_{open1_cytosol}$ $- k_{10} \times NRF2_{free_cytosol} + k_{11} \times NRF2_{free_nucleus} \times \frac{V_n}{V_c}$
2	Cytosolic free KEAP1 dimer	$\frac{dKEAP1_{free_cytosol}}{dt}$	=	$- 2 \times k_1 \times KEAP1_{free_cytosol} \times NRF2_{free_cytosol} + k_2 \times KEAP1_NRF2_{open1_cytosol}$ $- 2 \times k_7 \times KEAP1_{free_cytosol} \times CLASS_{VI} + k_8 \times CLASS_{VI_KEAP1_cytosol} + k_6 \times KEAP1_NRF2_{closed_cytosol}$ $+ k_9 \times KEAP1_NRF2_{open1_cytosol} + k_{9.1} \times KEAP1_NRF2_{open2_cytosol}$
3	Cytosolic single ClassVI-bound KEAP1 dimer	$\frac{dCLASS_{VI_KEAP1}_{cytosol}}{dt}$	=	$- k'_1 \times CLASS_{VI_KEAP1_cytosol} \times NRF2_{free_cytosol} + k'_2 \times CLASS_{VI_KEAP1_NRF2}_{open1_cytosol}$ $+ 2 \times k_7 \times KEAP1_{free_cytosol} \times CLASS_{VI} - k_8 \times CLASS_{VI_KEAP1_cytosol}$ $- k'_7 \times CLASS_{VI} \times CLASS_{VI_KEAP1_cytosol} + k'_8 \times CLASS_{VI2_KEAP1_cytosol}$ $+ k'_9 \times CLASS_{VI_KEAP1_NRF2}_{open1_cytosol} + k'_{9.1} \times CLASS_{VI_KEAP1_NRF2}_{open2_cytosol}$
4	Cytosolic dual ClassVI-bound KEAP1 dimer	$\frac{dCLASS_{VI2_KEAP1}_{cytosol}}{dt}$	=	$k'_7 \times CLASS_{VI} \times CLASS_{VI_KEAP1_cytosol} - k'_8 \times CLASS_{VI2_KEAP1_cytosol}$
5	Cytosolic intermediate open-state KEAP1-NRF2 complex	$\frac{dKEAP1_NRF2_{open1_cytosol}}{dt}$	=	$2 \times k_1 \times KEAP1_{free_cytosol} \times NRF2_{free_cytosol} - k_2 \times KEAP1_NRF2_{open1_cytosol} - k_{1.1} \times KEAP1_NRF2_{open1_cytosol}$ $+ k_{2.1} \times KEAP1_NRF2_{open2_cytosol} - k_7 \times CLASS_{VI} \times KEAP1_NRF2_{open1_cytosol}$ $+ k_8 \times CLASS_{VI_KEAP1_NRF2}_{open1_cytosol} - k_9 \times KEAP1_NRF2_{open1_cytosol}$
6	Cytosolic final open-state KEAP1-NRF2 complex	$\frac{dKEAP1_NRF2_{open2_cytosol}}{dt}$	=	$k_{1.1} \times KEAP1_NRF2_{open1} - k_{2.1} \times KEAP1_NRF2_{open2_cytosol} - k_3 \times KEAP1_NRF2_{open2_cytosol}$ $+ k_4 \times KEAP1_NRF2_{closed_cytosol} - k_7 \times CLASS_{VI} \times KEAP1_NRF2_{open2_cytosol}$ $+ k_8 \times CLASS_{VI_KEAP1_NRF2}_{open2_cytosol} - k_{9.1} \times KEAP1_NRF2_{open2_cytosol}$
7	Cytosolic closed-state KEAP1-NRF2 complex	$\frac{dKEAP1_NRF2_{closed_cytosol}}{dt}$	=	$k_3 \times KEAP1_NRF2_{open2_cytosol} - k_4 \times KEAP1_NRF2_{closed_cytosol} - k_6 \times KEAP1_NRF2_{closed_cytosol}$
8	Cytosolic intermediate open-state ClassVI-KEAP1-NRF2 complex	$\frac{dCLASS_{VI_KEAP1_NRF2}_{open1_cytosol}}{dt}$	=	$k'_1 \times CLASS_{VI_KEAP1_cytosol} \times NRF2_{free_cytosol} - k'_2 \times CLASS_{VI_KEAP1_NRF2}_{open1_cytosol}$ $- k'_{1.1} \times CLASS_{VI_KEAP1_NRF2}_{open1_cytosol} + k'_{2.1} \times CLASS_{VI_KEAP1_NRF2}_{open2_cytosol}$ $+ k_7 \times CLASS_{VI} \times KEAP1_NRF2_{open1_cytosol} - k_8 \times CLASS_{VI_KEAP1_NRF2}_{open1_cytosol}$ $- k'_9 \times CLASS_{VI_KEAP1_NRF2}_{open1_cytosol}$
9	Cytosolic intermediate open-state ClassVI-KEAP1-NRF2 complex	$\frac{dCLASS_{VI_KEAP1_NRF2}_{open2_cytosol}}{dt}$	=	$k'_{1.1} \times CLASS_{VI_KEAP1_NRF2}_{open1_cytosol} - k'_{2.1} \times CLASS_{VI_KEAP1_NRF2}_{open2_cytosol}$ $+ k_7 \times CLASS_{VI} \times KEAP1_NRF2_{open2_cytosol} - k_8 \times CLASS_{VI_KEAP1_NRF2}_{open2_cytosol}$ $- k'_{9.1} \times CLASS_{VI_KEAP1_NRF2}_{open2_cytosol}$
10	Nuclear free NRF2	$\frac{dNRF2_{free_nucleus}}{dt}$	=	$k_{10} \times NRF2_{free_cytosol} \times \frac{V_c}{V_n} - k_{11} \times NRF2_{free_nucleus} - k_{n5} \times NRF2_{free_nucleus}$ $- 2 \times k_{n1} \times NRF2_{free_nucleus} \times KEAP1_{free_nucleus} + k_{n2} \times KEAP1_NRF2_{open1_nucleus}$
11	Nuclear free KEAP1 dimer	$\frac{dKEAP1_{free_nucleus}}{dt}$	=	$- 2 \times k_{n1} \times NRF2_{free_nucleus} \times KEAP1_{free_nucleus} + k_{n2} \times KEAP1_NRF2_{open1_nucleus}$ $+ k_{n6} \times KEAP1_NRF2_{closed_nucleus} + k_{n9} \times KEAP1_NRF2_{open1_nucleus} + k_{n9.1} \times KEAP1_NRF2_{open2_nucleus}$

12	Nuclear intermediate open-state KEAP1-NRF2 complex	$\frac{dKEAP1_NRF2_{open1_nucleus}}{dt} = 2 \times k_{n1} \times NRF2_{free_nucleus} \times KEAP1_{free_nucleus} - k_{n2} \times KEAP1_NRF2_{open1_nucleus} - k_{n1.1} \times KEAP1_NRF2_{open1_nucleus} + k_{n2.1} \times KEAP1_NRF2_{open2_nucleus} - k_{n9} \times KEAP1_NRF2_{open1_nucleus}$
----	--	---

13	Nuclear final open-state KEAP1-NRF2 complex	$\frac{dKEAP1_NRF2_{open2_nucleus}}{dt} = k_{n1.1} \times KEAP1_NRF2_{open1_nucleus} - k_{n2.1} \times KEAP1_NRF2_{open2_nucleus} - k_{n3} \times KEAP1_NRF2_{open2_nucleus} + k_{n4} \times KEAP1_NRF2_{closed_nucleus} - k_{n9.1} \times KEAP1_NRF2_{open2_nucleus}$
----	---	--

14	Nuclear closed-state KEAP1-NRF2 complex	$\frac{dKEAP1_NRF2_{closed_nucleus}}{dt} = k_{n3} \times KEAP1_NRF2_{open2_nucleus} - k_{n4} \times KEAP1_NRF2_{closed_nucleus} - k_{n6} \times KEAP1_NRF2_{closed_nucleus}$
----	---	--

Table S7. Algebraic equations**Cytosolic total NRF2**

Models 1-2: $NRF2_{tot_cytosol} = NRF2_{free_cytosol} + KEAP1_NRF2_{open_cytosol} + KEAP1_o_NRF2_{open_cytosol} + KEAP1_NRF2_{closed_cytosol} + KEAP1_o_NRF2_{closed_cytosol}$

Models 3a-4b: $NRF2_{tot_cytosol} = NRF2_{free_cytosol} + KEAP1_NRF2_{open1_cytosol} + KEAP1_o_NRF2_{open1_cytosol} + KEAP1_NRF2_{open2_cytosol} + KEAP1_o_NRF2_{open2_cytosol} + KEAP1_NRF2_{closed_cytosol} + KEAP1_o_NRF2_{closed_cytosol}$

Nuclear total NRF2

Models 4a-4b: $NRF2_{tot_nucleus} = NRF2_{free_nucleus} + KEAP1_NRF2_{open1_nucleus} + KEAP1_NRF2_{open2_nucleus} + KEAP1_NRF2_{closed_nucleus}$

Cellular total NRF2

Models 4a-4b: $NRF2_{tot_cell} = \frac{NRF2_{tot_cytosol} \times V_c + NRF2_{tot_nucleus} \times V_n}{V_c + V_n}$

Cytosolic free KEAP1 dimer

Models 1, 2, 3a, 4a: $KEAP1_{free_cytosol} = KEAP1_{free_cytosol} + KEAP1_o_free_cytosol$

Cytosolic total open-state KEAP1-NRF2 complex

Models 1-2: $KEAP1_NRF2_{open_tot_cytosol} = KEAP1_NRF2_{open_cytosol} + KEAP1_o_NRF2_{open_cytosol}$

Models 3a and 4a: $KEAP1_NRF2_{open1_tot_cytosol} = KEAP1_NRF2_{open1_cytosol} + KEAP1_o_NRF2_{open1_cytosol}$

Models 3a and 4a: $KEAP1_NRF2_{open2_tot_cytosol} = KEAP1_NRF2_{open2_cytosol} + KEAP1_o_NRF2_{open2_cytosol}$

Models 3a and 4a: $KEAP1_NRF2_{open_tot_cytosol} = KEAP1_NRF2_{open1_cytosol} + KEAP1_o_NRF2_{open1_cytosol} + KEAP1_NRF2_{open2_cytosol} + KEAP1_o_NRF2_{open2_cytosol}$

Models 3b and 4b: $KEAP1_NRF2_{open1_tot_cytosol} = KEAP1_NRF2_{open1_cytosol} + CLASS_{VI_KEAP1_NRF2_{open1_cytosol}}$

Models 3b and 4b: $KEAP1_NRF2_{open2_tot_cytosol} = KEAP1_NRF2_{open2_cytosol} + CLASS_{VI_KEAP1_NRF2_{open2_cytosol}}$

Models 3b and 4b: $KEAP1_NRF2_{open_tot_cytosol} = KEAP1_NRF2_{open1_cytosol} + CLASS_{VI_KEAP1_NRF2_{open1_cytosol}} + KEAP1_NRF2_{open2_cytosol} + CLASS_{VI_KEAP1_NRF2_{open2_cytosol}}$

Cytosolic total closed-state KEAP1-NRF2 complex

Models 1, 2, 3a, 4a: $KEAP1_NRF2_{closed_tot_cytosol} = KEAP1_NRF2_{closed_cytosol} + KEAP1_o_NRF2_{closed_cytosol}$

Models 3b and 4b: $KEAP1_NRF2_{closed_tot_cytosol} = KEAP1_NRF2_{closed_cytosol}$

Table S8. Basal steady-state concentrations of NRF2 and KEAP1 species (nM)

Model #	KEAP1 _{free}	NRF2 _{free}	KEAP1_ NRF2 _{open1_tot}	KEAP1_ NRF2 _{open2_tot}	KEAP1_ NRF2 _{open_tot}	KEAP1_ NRF2 _{closed_tot}	KEAP1 _{tot}	NRF2 _{tot}
Cytosol								
1-2	382	2	na		74	74	530	150
3a-4b	386	6.2	58	14	72	72		
Nucleus								
4a-4b	2.6	180	11.5	14	25.5	72	100	278

Note: na: not applicable. Due to rounding, values may not add up exactly.

Table S9. Maximally induced steady-state concentrations of NRF2 and KEAP1 species (nM)

Model #	KEAP1 _{free}	NRF2 _{free}	KEAP1_ NRF2 _{open1_tot}	KEAP1_ NRF2 _{open2_tot}	KEAP1_ NRF2 _{open_tot}	KEAP1_ NRF2 _{closed_tot}	KEAP1 _{tot}	NRF2 _{tot}
Cytosol								
1	11.2	231	na		258	260	530	750
2	2.82	223	na		63	465		
3a	6.62	227	36	80	116	407		
3b	2.65E-8	519	0.033	0.187	0.22	9.46E-6		
4a	68	19	32	70	102	359		
4b	2.65E-8	33	2.13E-3	0.012	0.014	6.02E-7		
Nucleus								
4a	0.77	626	12	14	26	73	100	725
4b	0.45	1079	12	14	26	73		

Note: Maximal induction is achieved by setting CLASS_{1,v} or CLASS_{v1} to 10E6. na: not applicable. Due to rounding, values may not add up exactly.

Table S10. Basal turnover fluxes of KEAP1-NRF2 models (nM/S)

Model #	flux _{k0}	flux _{k1}	flux _{k2}	flux _{k1,1}	flux _{k2,1}	flux _{k3}	flux _{k4}	flux _{k5}	flux _{k6}	flux _{k9}	flux _{k9,1}	flux _{k10}	flux _{k11} *
1	0.172	21.078	20.906	na	14.645	14.495	5.65E-4	0.1501	0.0214			na	
2	0.15	21.116	20.966	na	0.1353	7.35E-3	5.66E-4	0.128	0.0215			na	
3a-3b	0.15	16.482	16.334	0.1332	1.73E-3	14.194	14.066	1.78E-3	0.1274	1.67E-3	4.1E-3	na	
4a-4b	0.1933	Same as Models 3a-3b										0.1185	0.0751

Note: *: normalized to cytosolic volume; na: not applicable. Due to rounding, values may not add up exactly.

Table S11. Maximally-induced turnover fluxes of KEAP1-NRF2 models (nM/S)

Model #	flux _{k0}	flux _{k1} + flux _{k'1}	flux _{k2} + flux _{k'2}	flux _{k1,1} + flux _{k'1,1}	flux _{k2,1} + flux _{k'2,1}	flux _{k3} + flux _{k'3} #	flux _{k4} + flux _{k'4} #	flux _{k5}	flux _{k6}	flux _{k'6}	flux _{k9} + flux _{k'9}	flux _{k9,1} + flux _{k'9,1}	flux _{k10}	flux _{k11} *
1	0.172	72.99	72.89	na	51.06	51.03	0.067	5.3E-6	0.031	0.075			na	
2	0.15	17.75	17.66	na	0.114	0.046	0.064	8.1E-6	0.068	0.018			na	
3a	0.15	10.36	10.27	0.084	9.7E-3	79.84	79.79	0.065	7.2E-6	0.051	0.011	0.023	na	
3b	0.15	9.5E-3	9.4E-3	7.7E-5	2.3E-5	1.87E-6	1.85E-6	0.15	1.7E-8	na	9.7E-6	5.4E-5	na	
4a	0.1933	9.141	9.067	0.074	8.6E-3	70.48	70.43	5.6E-3	6.4E-6	0.045	9.3E-3	0.02	0.373	0.26
4b	0.1933	6.0E-4	6.0E-4	4.9E-6	1.5E-6	1.19E-7	1.18E-7	9.5E-3	1.0E-9	na	6.1E-7	3.4E-6	0.632	0.449

Note: Maximal induction is achieved by setting CLASS_{1,v} or CLASS_{v1} to 10E6. #: flux_{k3} and flux_{k'3} do not exist for Models 3b and 4b; *: normalized to cytosolic volume; na: not applicable. Due to rounding, values may not add up exactly.

Table S12. Classes of electrophilic and non-electrophilic NRF2 activators

Activators	Reactive Cysteines	Representative Chemicals	References
Class I	Cys151	DEM, 1,2-NQ, SFN, SNAP, CDDOIm, DMF, NO, tBHQ	<i>Kobayashi et al. 2009, Saito et al. 2016, Suzuki and Yamamoto 2017</i>
Class II	Cys288	15d-PGJ ₂	<i>Levonen et al. 2004, Kobayashi et al. 2009, Saito et al. 2016</i>
Class III	Cys151/Cys273/Cys288	As ³⁺ , 4-HNE, 9-OA-NO ₂	<i>McMahon et al. 2010, Saito et al. 2016</i>
Class IV	Cys226/Cys613/Cys622/Cys624	H ₂ O ₂ , Cd ²⁺ , AF	<i>McMahon et al. 2010, Suzuki et al. 2019</i>
Class V	Cys257/Cys319/Cys434/Cys489	PGA ₂ , Ebselen	<i>Suzuki et al. 2019</i>
Class VI	Not applicable	p62, Cpd16, FAM129B	<i>Komatsu et al. 2010, Lau et al. 2010, Jiang et al. 2014, Cheng et al. 2019</i>

References:

Alam, J., E. Killeen, P. Gong, R. Naquin, B. Hu, D. Stewart, J. R. Ingelfinger and K. A. Nath (2003). "Heme activates the heme oxygenase-1 gene in renal epithelial cells by stabilizing Nrf2." Am J Physiol Renal Physiol **284**(4): F743-752.

Baird, L., D. Llères, S. Swift and A. T. Dinkova-Kostova (2013). "Regulatory flexibility in the Nrf2-mediated stress response is conferred by conformational cycling of the Keap1-Nrf2 protein complex." Proc Natl Acad Sci U S A **110**(38): 15259-15264.

Burroughs, A. F., S. Eluhu, D. Whalen, J. S. Goodwin, A. M. Sakwe and I. J. Arinze (2018). "PML-Nuclear Bodies Regulate the Stability of the Fusion Protein Dendra2-Nrf2 in the Nucleus." Cellular Physiology and Biochemistry **47**(2): 800-816.

Chen, Y., D. Inoyama, A. N. Kong, L. J. Beamer and L. Hu (2011). "Kinetic analyses of Keap1-Nrf2 interaction and determination of the minimal Nrf2 peptide sequence required for Keap1 binding using surface plasmon resonance." Chem Biol Drug Des **78**(6): 1014-1021.

Cheng, K. C., R. J. Lin, J. Y. Cheng, S. H. Wang, J. C. Yu, J. C. Wu, Y. J. Liang, H. M. Hsu, J. Yu and A. L. Yu (2019). "FAM129B, an antioxidative protein, reduces chemosensitivity by competing with Nrf2 for Keap1 binding." EBioMedicine **45**: 25-38.

Chowdhry, S., Y. Zhang, M. McMahon, C. Sutherland, A. Cuadrado and J. D. Hayes (2013). "Nrf2 is controlled by two distinct β -TrCP recognition motifs in its Neh6 domain, one of which can be modulated by GSK-3 activity." Oncogene **32**(32): 3765-3781.

Crinelli, R., C. Zara, L. Galluzzi, G. Buffi, C. Ceccarini, M. Smietana, M. Mari, M. Magnani and A. Fraternali (2021). "Activation of NRF2 and ATF4 Signaling by the Pro-Glutathione Molecule I-152, a Co-Drug of N-Acetyl-Cysteine and Cysteamine." Antioxidants (Basel) **10**(2).

Eggler, A. L., G. Liu, J. M. Pezzuto, R. B. van Breemen and A. D. Mesecar (2005). "Modifying specific cysteines of the electrophile-sensing human Keap1 protein is insufficient to disrupt binding to the Nrf2 domain Neh2." Proc Natl Acad Sci U S A **102**(29): 10070-10075.

Fukutomi, T., K. Takagi, T. Mizushima, N. Ohuchi and M. Yamamoto (2014). "Kinetic, thermodynamic, and structural characterizations of the association between Nrf2-DLx1 and Keap1." Mol Cell Biol **34**(5): 832-846.

He, X., M. G. Chen, G. X. Lin and Q. Ma (2006). "Arsenic induces NAD(P)H-quinone oxidoreductase I by disrupting the Nrf2 x Keap1 x Cul3 complex and recruiting Nrf2 x Maf to the antioxidant response element enhancer." J Biol Chem **281**(33): 23620-23631.

Horie, Y., T. Suzuki, J. Inoue, T. Iso, G. Wells, T. W. Moore, T. Mizushima, A. T. Dinkova-Kostova, T. Kasai, T. Kamei, S. Koshiba and M. Yamamoto (2021). "Molecular basis for the disruption of Keap1-Nrf2 interaction via Hinge & Latch mechanism." Communications Biology **4**(1): 576.

Ichimura, Y., S. Waguri, Y. S. Sou, S. Kageyama, J. Hasegawa, R. Ishimura, T. Saito, Y. Yang, T. Kouno, T. Fukutomi, T. Hoshii, A. Hirao, K. Takagi, T. Mizushima, H. Motohashi, M. S. Lee, T. Yoshimori, K. Tanaka, M. Yamamoto and M. Komatsu (2013). "Phosphorylation of p62 activates the Keap1-Nrf2 pathway during selective autophagy." Mol Cell **51**(5): 618-631.

Iso, T., T. Suzuki, L. Baird and M. Yamamoto (2016). "Absolute Amounts and Status of the Nrf2-Keap1-Cul3 Complex within Cells." Mol Cell Biol **36**(24): 3100-3112.

Itoh, K., N. Wakabayashi, Y. Katoh, T. Ishii, T. O'Connor and M. Yamamoto (2003). "Keap1 regulates both cytoplasmic-nuclear shuttling and degradation of Nrf2 in response to electrophiles." Genes Cells **8**(4): 379-391.

Jiang, Z. Y., M. C. Lu, L. L. Xu, T. T. Yang, M. Y. Xi, X. L. Xu, X. K. Guo, X. J. Zhang, Q. D. You and H. P. Sun (2014). "Discovery of potent Keap1-Nrf2 protein-protein interaction inhibitor based on molecular binding determinants analysis." J Med Chem **57**(6): 2736-2745.

Khalil, H. S., A. Goltsov, S. P. Langdon, D. J. Harrison, J. Bown and Y. Deeni (2015). "Quantitative analysis of NRF2 pathway reveals key elements of the regulatory circuits underlying antioxidant response and proliferation of ovarian cancer cells." J Biotechnol **202**: 12-30.

Kobayashi, A., M. I. Kang, H. Okawa, M. Ohtsui, Y. Zenke, T. Chiba, K. Igarashi and M. Yamamoto (2004). "Oxidative stress sensor Keap1 functions as an adaptor for Cul3-based E3 ligase to regulate proteasomal degradation of Nrf2." Mol Cell Biol **24**(16): 7130-7139.

Kobayashi, A., M. I. Kang, Y. Watai, K. I. Tong, T. Shibata, K. Uchida and M. Yamamoto (2006). "Oxidative and electrophilic stresses activate Nrf2 through inhibition of ubiquitination activity of Keap1." Mol Cell Biol **26**(1): 221-229.

Kobayashi, M., L. Li, N. Iwamoto, Y. Nakajima-Takagi, H. Kaneko, Y. Nakayama, M. Eguchi, Y. Wada, Y. Kumagai and M. Yamamoto (2009). "The antioxidant defense system Keap1-Nrf2 comprises a multiple sensing mechanism for responding to a wide range of chemical compounds." Mol Cell Biol **29**(2): 493-502.

Komatsu, M., H. Kurokawa, S. Waguri, K. Taguchi, A. Kobayashi, Y. Ichimura, Y. S. Sou, I. Ueno, A. Sakamoto, K. I. Tong, M. Kim, Y. Nishito, S. Iemura, T. Natsume, T. Ueno, E. Kominami, H. Motohashi, K. Tanaka and M. Yamamoto (2010). "The selective autophagy substrate p62 activates the stress responsive transcription factor Nrf2 through inactivation of Keap1." Nat Cell Biol **12**(3): 213-223.

Kwak, M. K., K. Itoh, M. Yamamoto and T. W. Kensler (2002). "Enhanced expression of the transcription factor Nrf2 by cancer chemopreventive agents: role of antioxidant response element-like sequences in the nrf2 promoter." Mol Cell Biol **22**(9): 2883-2892.

Lau, A., X. J. Wang, F. Zhao, N. F. Villeneuve, T. Wu, T. Jiang, Z. Sun, E. White and D. D. Zhang (2010). "A noncanonical mechanism of Nrf2 activation by autophagy deficiency: direct interaction between Keap1 and p62." Mol Cell Biol **30**(13): 3275-3285.

Levonen, A. L., A. Landar, A. Ramachandran, E. K. Ceaser, D. A. Dickinson, G. Zanoni, J. D. Morrow and V. M. Darley-Usmar (2004). "Cellular mechanisms of redox cell signalling: role of cysteine modification in controlling antioxidant defences in response to electrophilic lipid oxidation products." Biochem J **378**(Pt 2): 373-382.

Lo, S. C., X. Li, M. T. Henzl, L. J. Beamer and M. Hannink (2006). "Structure of the Keap1:Nrf2 interface provides mechanistic insight into Nrf2 signaling." Embo j **25**(15): 3605-3617.

McMahon, M., D. J. Lamont, K. A. Beattie and J. D. Hayes (2010). "Keap1 perceives stress via

three sensors for the endogenous signaling molecules nitric oxide, zinc, and alkenals." Proc Natl Acad Sci U S A **107**(44): 18838-18843.

McMahon, M., N. Thomas, K. Itoh, M. Yamamoto and J. D. Hayes (2004). "Redox-regulated turnover of Nrf2 is determined by at least two separate protein domains, the redox-sensitive Neh2 degron and the redox-insensitive Neh6 degron." J Biol Chem **279**(30): 31556-31567.

Ogura, T., K. I. Tong, K. Mio, Y. Maruyama, H. Kurokawa, C. Sato and M. Yamamoto (2010). "Keap1 is a forked-stem dimer structure with two large spheres enclosing the intervening, double glycine repeat, and C-terminal domains." Proc Natl Acad Sci U S A **107**(7): 2842-2847.

Rada, P., A. I. Rojo, S. Chowdhry, M. McMahon, J. D. Hayes and A. Cuadrado (2011). "SCF/ β -TrCP promotes glycogen synthase kinase 3-dependent degradation of the Nrf2 transcription factor in a Keap1-independent manner." Mol Cell Biol **31**(6): 1121-1133.

Saito, R., T. Suzuki, K. Hiramoto, S. Asami, E. Naganuma, H. Suda, T. Iso, H. Yamamoto, M. Morita, L. Baird, Y. Furusawa, T. Negishi, M. Ichinose and M. Yamamoto (2016). "Characterizations of Three Major Cysteine Sensors of Keap1 in Stress Response." Mol Cell Biol **36**(2): 271-284.

Sasaki, K. and G. Matsumura (1989). "Mononuclear cells in the extraembryonic and intraembryonic coelom of the mouse embryo: a semithin light microscopic cytometry." Arch Histol Cytol **52**(4): 421-426.

Stewart, D., E. Killeen, R. Naquin, S. Alam and J. Alam (2003). "Degradation of transcription factor Nrf2 via the ubiquitin-proteasome pathway and stabilization by cadmium." J Biol Chem **278**(4): 2396-2402.

Suzuki, T., A. Muramatsu, R. Saito, T. Iso, T. Shibata, K. Kuwata, S. I. Kawaguchi, T. Iwawaki, S. Adachi, H. Suda, M. Morita, K. Uchida, L. Baird and M. Yamamoto (2019). "Molecular Mechanism of Cellular Oxidative Stress Sensing by Keap1." Cell Rep **28**(3): 746-758 e744.

Suzuki, T. and M. Yamamoto (2017). "Stress-sensing mechanisms and the physiological roles of the Keap1-Nrf2 system during cellular stress." J Biol Chem **292**(41): 16817-16824.

Tong, K. I., Y. Katoh, H. Kusunoki, K. Itoh, T. Tanaka and M. Yamamoto (2006). "Keap1 recruits Neh2 through binding to ETGE and DLG motifs: characterization of the two-site molecular recognition model." Mol Cell Biol **26**(8): 2887-2900.